Astronomy & Astrophysics manuscript no. ENHANCED
November 3, 2014

The impact of mass-loss on the evolution and pre-supernova properties of red supergiants

G. Meynet[1], V. Chomienne[1], S. Ekström[1], C. Georgy[2], A. Granada[1], J. Groh[1], A. Maeder[1], P. Eggenberger[1], E. Levesque[3] and P. Massey[4]

[1] Geneva Observatory, University of Geneva, Maillettes 51, CH-1290 Sauverny, Switzerland
[2] Astrophysics, Lennard-Jones Laboratories, EPSAM, Keele University, Staffordshire ST5 5BG, UK
[3] CASA, Department of Astrophysical and Planetary Sciences, University of Colorado 389-UCB, Boulder, CO 80309, USA
[4] Lowell Observatory, 1400 W Mars Hill Road, Flagstaff, AZ 86001, USA

Received ; accepted

ABSTRACT

Context. The post main-sequence evolution of massive stars is very sensitive to many parameters of the stellar models. Key parameters are the mixing processes, the metallicity, the mass-loss rate and the effect of a close companion.
Aims. We study how the red supergiant lifetimes, the tracks in the Hertzsprung-Russel diagram (HRD), the positions in this diagram of the pre-supernova progenitor as well as the structure of the stars at that time change for various mass-loss rates during the red supergiant phase (RSG), and for two different initial rotation velocities.
Methods. Stellar models are computed with the Geneva code for initial masses between 9 and 25 $M_\odot$ at solar metallicity (Z=0.014) with 10 times and 25 times the standard mass-loss rates during the red supergiant phase, with and without rotation.
Results. The surface abundances of RSGs are much more sensitive to rotation than to the mass-loss rates during that phase. A change of the RSG mass-loss rate has a strong impact on the RSG lifetimes and therefore on the luminosity function of RSGs. An observed RSG is associated to a larger initial mass model, when enhanced RSG mass-loss rate models are used to deduce that mass. At solar metallicity, the enhanced mass-loss rate models do produce significant changes on the populations of blue, yellow and red supergiants. When extended blue loops or blue ward excursions are produced by enhanced mass-loss, the models predict that a majority of blue (yellow) supergiants are post RSG objects. These post RSG stars are predicted to show much smaller surface rotational velocities than similar blue supergiants on their first crossing of the HR gap. Enhanced mass-loss rates during the red supergiant phase has little impact on the Wolf-Rayet (WR) populations. The position in the HRD of the end point of the evolution depends on the mass of the hydrogen envelope. More precisely, whenever, at the pre-supernova stage, the H-rich envelope contains more than about 5% of the initial mass, the star is a red supergiant, and whenever the H-rich envelope contains less than 1% of the total mass the star is a blue supergiant. For intermediate situations, intermediate colors/effective temperatures are obtained. Yellow progenitors for core collapse supernovae can be explained by the enhanced mass-loss rate models, while the red progenitors are better fitted by the standard mass-loss rate models.

Key words. stars: general – stars: evolution – stars: rotation

1. Introduction

Red supergiants (RSG) represent a long-lasting stage during the core He-burning stage of all massive stars with masses between about 9 and 25 $M_\odot$. Therefore, a large number of post-Main Sequence massive stars are expected to be in this evolutionary stage. This kind of stars represent the end point of the evolution of about half of the massive stars. When such a star core-collapses, it produces a type II-P or type II-L supernova event. Interactions of the supernova ejecta with the dense red supergiant wind may in some circumstances produce type II-n supernovae (see e.g. Smith et al. 2011). These stars are the progenitors of neutron stars and maybe also of some black holes. Thanks to their high luminosities, they can be observed far away in the Universe and used to probe, for instance, the metallicity of distant galaxies (Davies et al. 2010). For all these reasons, red supergiants represent key objects to understand.

While models can reproduce satisfactorily some observed properties of red supergiants as for instance their positions in the HR diagrams (Levesque et al. 2005, 2006; Massey et al. 2009), these stars also pose some interesting questions. For instance, are all red supergiants exploding in a type II core collapse event? Or do some of them represent a transitory stage before the star evolves back to bluer regions of the HR diagram (Yoon & Cantiello 2010; Georgy et al. 2012; Georgy 2012; Groh et al. 2013a,b)? Can such further evolution explain the high number of blue supergiants observed in solar metallicity clusters with mass at the turn off around 9-15 $M_\odot$ (Meylan & Maeder 1983; Eggenberger et al. 2002), the low-luminosity WC stars (Georgy et al. 2012), low-luminosity luminous blue variables (LBV) as SN progenitors (Groh et al. 2013a) and/or the yellow supergiants progenitors of core collapse events (Georgy 2012), as for instance 2011dh (Van Dyk et al. 2013)?

Actually all these questions are somewhat intertwined and should be addressed simultaneously. This is what we want to do in the present paper, focusing on solar metallicity models. A key point for answering these questions is a good knowledge of the mass-loss rates during the RSG phase. Unfortunately this quantity is not well constrained observationally (see the discussion in the next section). The difficulty to deduce the mass-loss rates during the RSG phase comes from the complexity of the

envelopes of these stars and thus from the difficulty to obtain reliable spectroscopic diagnostics. Moreover, it is likely that these stars do not lose mass uniformly as a function of time but undergo strong and short outbursts. One spectacular example is VY CMa. It is a luminous M supergiant with a luminosity equal to 2-3 $\times$ 10^5 $L_\odot$ for the parallax distance of 1.14±0.09 kpc (see Choi et al. 2008). The star has a dusty circumstellar envelope (Humphreys et al. 2007) which produces a reflection nebula at optical wavelengths. Smith et al. (2001) estimate the mass of the nebula surrounding VY CMa as 0.2-0.4 $M_\odot$. Decin et al. (2006) deduced that VY CMa had undergone a phase of high mass-loss (about 3.2×10^{-4} $M_\odot$ yr^{-1}) some 1000 years ago (see Fig. 1).

If this outbursting mode of losing mass was common among red supergiants, then this would make their modeling quite difficult [1]. Even with reliable spectroscopic diagnostics of the current mass-loss rate, our vision might be biased towards mass-loss rate values representative of the long periods when the star is in a weak wind regime. We may miss the much more seldom and short mass-loss episodes during which most of the mass might be lost. Moreover, we have at present no firm theory for making predictions on the frequency and the durations of such outbursts, although some authors have proposed that they may be triggered by pulsations (Yoon & Cantiello 2010). So, at the moment, the most promising way to make progress is to compute models with various mass-loss rates during the RSG stage and to see whether some range of mass-losses seem to be preferred over others to predict some peculiar outcomes. This is the aim of the present work, where we build on initial efforts from Georgy (2012) that focused on the pre-SN phase.

In Sect. 2 we present the physical ingredients of our stellar models. Section 3 discusses the impact of different RSG mass-loss rates on the evolutionary tracks and lifetimes. The impacts on the properties of the RSG and of the post-RSG are investigated in Sects. 4 and 5 respectively. Implications for the populations of Wolf-Rayet, blue, yellow and red supergiants are discussed in Sect. 6. Conclusions and perspectives are presented in Sect. 7.

2. The stellar models

Except for the mass-loss rates in the non-standard cases (see below), the models are computed with exactly the same physical ingredients as the models computed by Ekström et al. (2012), so the interested reader can refer to that paper for a detailed account. Let us just recall here that the models are computed with the Schwarzschild criteria for convection with a core overshooting. The core extension due to overshooting is taken equal to 10% the pressure scale height estimated at the Schwarzschild core boundary. Non adiabatic convection is considered in the outer convective zone with a mixing length scale equals to 1.6 times the local pressure scale height. In rotating models, the shear turbulence coefficient is taken from Maeder (1997), while the horizontal turbulence and the effective diffusion coefficients are those from Zahn (1992).

The mass-loss prescription for the hot part of the evolutionary tracks is that of de Jager et al. (1988) for the initial masses 9 and 15 $M_\odot$ and for Log $(T_{\rm eff}/K) > 3.7$. For Log $(T_{\rm eff}/K) < 3.7$, we use a fit on the data by Sylvester et al. (1998) and van Loon et al. (2005) as suggested by Crowther (2001). Above 15 $M_\odot$, the prescription given by Vink et al. (2001) is used on the MS phase as long as Log $(T_{\rm eff}/K) > 3.9$, the recipe from de Jager et al. (1988) is used for the non red supergiant phase. For Log $(T_{\rm eff}/K) < 3.7$, the prescription is the same as for lower initial mass stars. The effects of rotation on the mass-loss rates are accounted for as in Maeder & Meynet (2000). Note that these effects are quite negligible for the rotation rates considered in this work.

As explained in Ekström et al. (2012), for massive stars ($> 15\,M_\odot$) in the red supergiant phase, some points in the most external layers of the stellar envelope might exceed the Eddington luminosity of the star: $L_{\rm Edd} = 4\pi cGM/\kappa$ (with κ the opacity). This is due to the opacity peak produced by the variation of the ionization level of hydrogen beneath the surface of the star. We account for this phenomenon by increasing the mass-loss rate of the star (computed according to the prescription described above) by a factor of 3. Once the supra-Eddington layers disappear, later during the evolution, we come back to the usual mass-loss rate. Adopting this factor 3 in case of supra-Eddington luminosity layers and the mass loss recipes indicated above produces the standard time-averaged mass loss rates shown by the heavy continuous lines in Fig. 1. One sees that it well goes along the average mass loss rate determinations for RSG's by various authors.

For the enhanced mass-loss rate models, we just multiply by a factor 10 or 25 the mass-loss rates as given by the prescriptions indicated above during the whole period when the star is a RSG. We consider the star is a RSG when its effective temperature ($T_{\rm eff}$), as estimated by the Geneva code, is $\log(T_{\rm eff}/K) < 3.7$. We chose this limit because for every stellar models considered here, it encompasses the evolutionary phase during which the tracks become vertical in the HR diagram. Although this is a slightly too high $T_{\rm eff}$ for RSGs, using a smaller limiting value such as $\log(T_{\rm eff}/K) < 3.6$ would not have changed our results. This is because the part of the evolution comprised between $\log(T_{\rm eff}/K) = 3.6$ and 3.7 is very short compared to the time spent with $\log(T_{\rm eff}/K) < 3.6$. Note that when these enhanced mass loss rates are used, we do not account for the effect of the supra-Eddington layers as described in Ekström et al. (2012). This means that the enhancement of the mass-loss rates with respect to those used in Ekström et al. (2012) are actually a little less than the factor 10 and 25. The reader can look at Fig. 1 to get an idea of the enhancement factor with respect to the mass loss rate used in Ekström et al. (2012).

The enhancement factors of 10 and 25 are chosen somewhat arbitrarily. The only guideline we considered were to not overcome the maximum mass loss rates estimated by van Loon et al. (2005) (see the empty circles in Fig. 1). We could have explored also the cases of mass loss rates lower than those indicated by the continuous line in Fig. 1. In that case, the differences with respect to the standard tracks presented here would be mainly an increase of the maximum initial mass of stars that end their lifetimes as RSGs. The cases with enhanced mass loss rates are the most interesting to study since they can propose a solution for those stars, in the mass range between 9 and 25 $M_\odot$, ending their lifetimes as yellow, blue or even Wolf-Rayet stars, moreover such models somewhat mimics what would be the evolution in case of strong mass losses, during the RSG phase, triggered by a mass transfer in a close binary system. That is why we concentrate on those models in the present work.

[1] Note that strong mass losses may also be triggered by mass transfer in a close binary system during the RSG phase. Our enhanced mass-loss rate models during the RSG phase may mimic such a situation.

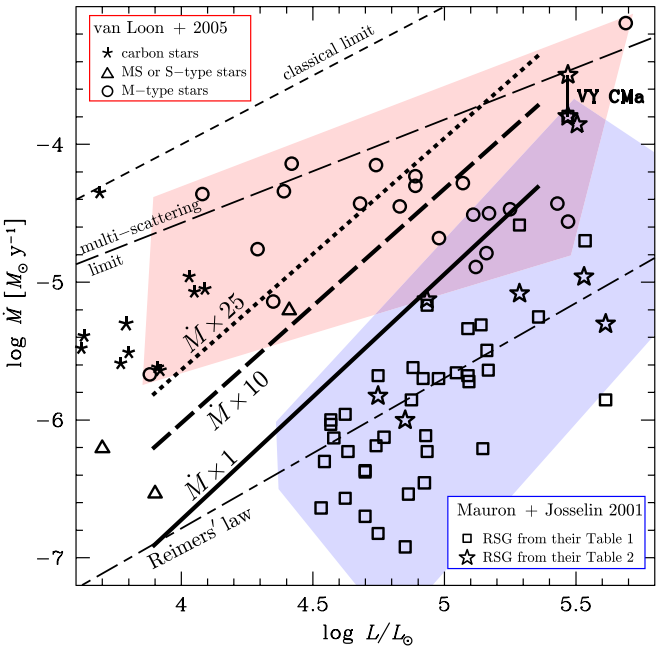

Fig. 1. Comparison between the mass-loss rates deduced from spectroscopy by different authors and the average values used in our models during the red supergiant phase. The data by van Loon et al. (2005) cover the region shaded in red. The data by Mauron & Josselin (2011) are distributed in the region shaded in blue. The two stars linked by a vertical line show the mass-loss rates for VY CMa; the lower value is taken from the table 1 of Mauron & Josselin (2011), the upper one is from Matsuura et al. (2014).The heavy continuous, long-dashed and dotted lines are our averaged red supergiant mass-loss rates equal to respectively 1, 10 and 25 times the standard mass-loss rate (see text). The upper thin long and short-dashed slanted lines mark the classical and multiple-scattering limits to the mass-loss rate (van Loon et al. 1999). The lower thin short-long-dashed line shows the Reimers law for an average temperature $T_{\rm eff}$= 3750 K (see Mauron & Josselin 2011).

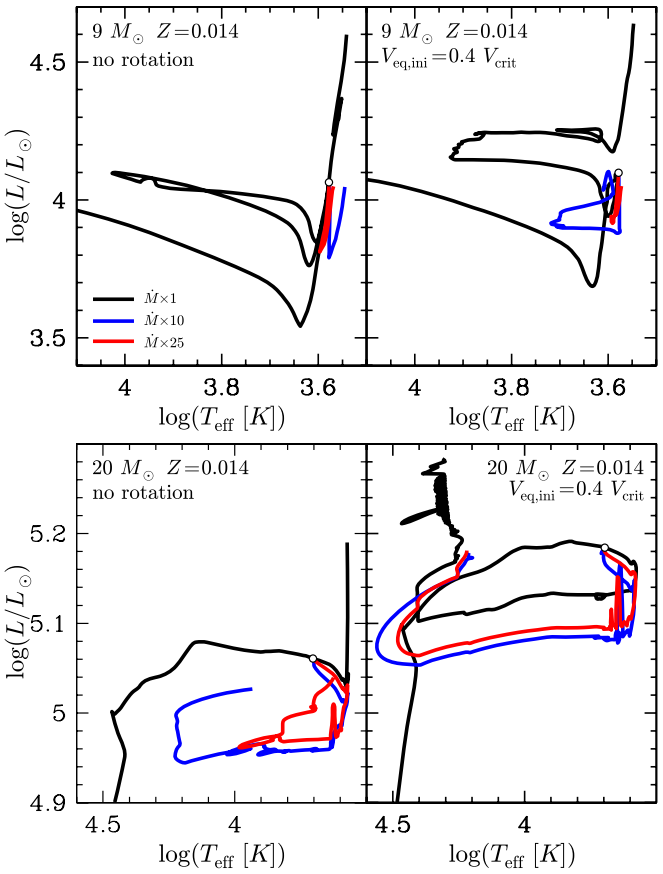

Fig. 2. Evolutionary tracks for the 9 and 20 $M_\odot$ stellar models for various prescriptions of the RSG mass-loss rates. Only partial tracks are shown. In the upper panel, the lowest line shows the first crossing from blue to red of the HR gap. The beginning of the portion of the track computed with an enhanced RSG mass-loss rate is indicated by a small empty circle.

2.1. Comparisons with spectroscopically determined mass-loss rates

We can wonder whether these enhancement factors for the mass-loss rates are compatible with spectroscopically determined mass-loss rates. In Fig. 1, mass-loss rate determinations for red supergiant stars are shown as a function of their luminosity. The low (blue) shaded area covers the region where the sample of stars examined by Mauron & Josselin (2011, see their Tables 1 and 2) are located, while the upper (red) shaded area shows the region covered by the dust-enshrouded red supergiants studied by van Loon et al. (2005). We can see that at a given luminosity, the scatter of the mass-loss rates is very high as already noted by Jura & Kleinmann (1990) and Josselin et al. (2000). At a given luminosity, the mass-loss rates can show values which can differ by more than two orders of magnitude!

Is this very large scatter real or due to uncertainties in the techniques used to infer the mass-loss rates? In this work we assume that a significant part of that scatter is real. In Fig. 1, we compare the observationally deduced mass-loss rates with the time averaged mass-loss rates obtained in the present work during the red supergiant phase (see the heavy lines). The averaged mass-loss rates have been obtained by simply extracting from the models the total mass lost and the duration of the RSG phase (see the numbers in Table 1). We estimated also for each initial mass model the time averaged luminosity during the RSG phase. We see that, 1) the RSG mass-loss rate for the reference models (those of Ekström et al. 2012), more or less go through the middle of the distribution of the points, indicating that this choice of the mass-loss rate may be a good one for representing the averaged evolution; 2) the models with mass-loss rates enhanced by a factor 10 and even 25 remain in a domain of mass-loss rates compatible with the mass-loss rates deduced from spectroscopy.

3. Evolutionary tracks and RSG lifetimes

The impact of the changes of the mass-loss rates during the red supergiant phase on the evolutionary tracks of the 9 and 20 $M_\odot$ models are shown in Fig 2. One observes that in the case of the 9 $M_\odot$ model, the enhancement of the red supergiant mass-loss rate suppresses the blue loop, hence increasing the time spent in the red supergiant phase, while for the 20 $M_\odot$, the mass-loss rate enhancement has the opposite effect. Rotation does not change qualitatively these trends [2].

Why does an increase in the mass-loss rate of the 9 $M_\odot$ reduce or even suppress the blue loop, while for the 20 $M_\odot$, on the contrary, it favors a blue ward evolution? The physics of the blue ward evolution is not the same in the 9 and the 20 $M_\odot$ model.

[2] Actually, rotation produces marginal changes on the red supergiant lifetimes for the 9 $M_\odot$ stellar model (see Fig. 3), while it reduces the RSG lifetime by a little more than 0.2 dex for the 20 $M_\odot$ model. This is mainly due to the fact that the rotating models have higher luminosities, therefore suffer stronger mass-losses which reduce the RSG lifetimes.

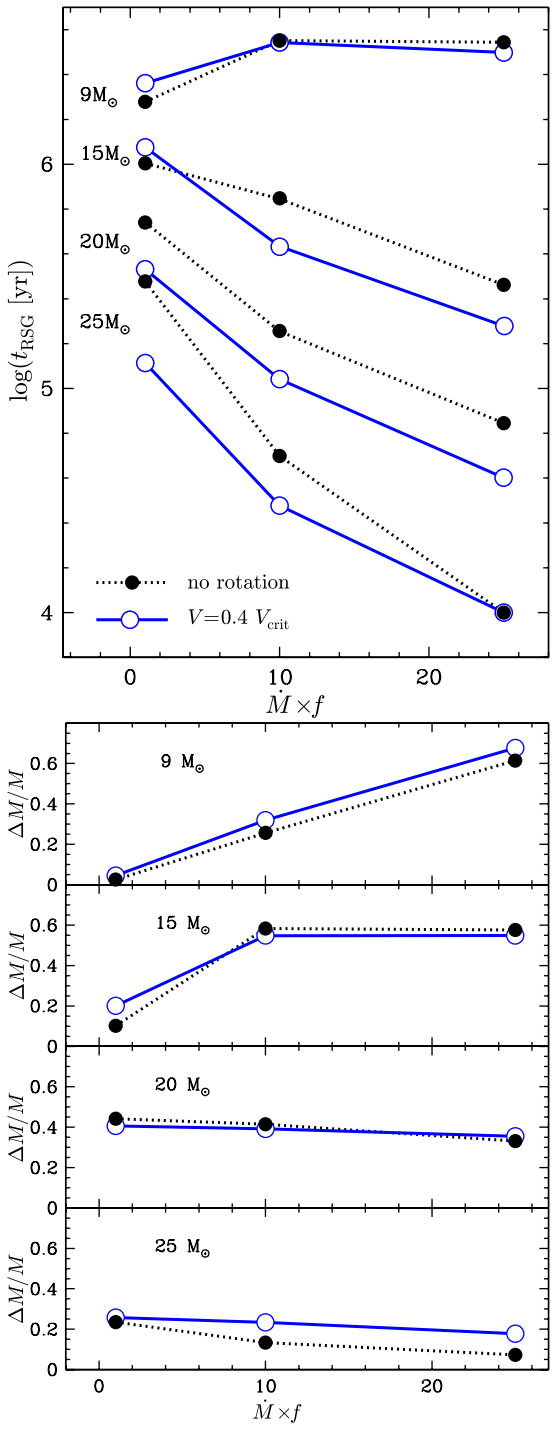

Fig. 3. *Upper panel:* Logarithm of the red supergiant lifetimes as a function of the enhancement factor for the mass-loss rate during the red supergiant phase. *Lower panel:* Fraction of the initial mass lost during the RSG phase, $\Delta M/M$, as a function of the enhancement factor of the RSG mass-loss rate (see text).

In the case of the 20 $M_\odot$, what makes the star evolve to the blue when the mass-loss increases is the fact that the star becomes more and more homogenous, the helium core representing a still larger part of the total mass of the star (Giannone 1967). Typically, when the mass fraction of the He-core becomes greater than about 60-70% of the total actual mass (this limiting fraction depends on the initial mass of the model considered), the star evolves back to the blue part of the HR diagram.

For the 9 $M_\odot$, we have a different situation. What makes the star to evolve back to the blue is the fact that, at some stage during the core helium burning phase, the core expands, implying by mirror effect, a contraction of the envelope. An expansion of the core occurs more easily in a model which has a not too much massive core. Lauterborn et al. (1971) have shown that for such stars, the red-blue motion in the HR diagram mainly depends on the gravitational potential of the He-core, $\Phi_{\rm core}$ and how it compares with some critical potential $\Phi_{\rm crit}(M)$ which grows with the stellar mass. One has that when the gravitational potential of the He-core is greater than this critical potential, then the star remains in the RSG stage, while, when it is smaller, the core can expand and the envelope contracts, and the star reaches a blue location in the HR diagram. So we can write

$$\Phi_{\rm core} > \Phi_{\rm crit}(M) \quad \text{Hayashi line,}$$

$$\Phi_{\rm core} < \Phi_{\rm crit}(M) \quad \text{blue location.}$$

For masses equal or above 15 $M_\odot$, we are in the first situation, for the 9 $M_\odot$, in the second one.

When the mass loss rates increase, for the 9 $M_\odot$ model, this decreases $\Phi_{\rm crit}(M)$. This favors the case where $\Phi_{\rm core} > \Phi_{\rm crit}(M)$, and an evolution keeping the star in the red part of the HR diagram. For the more massive stars, an increase of the mass loss rates also disfavors the evolution back to the blue due to the mirror effect. But as explained above, these stars may nevertheless evolve back to the blue because due to their massive convective cores, when mass loss is strong, the structure of the star becomes more and more homogeneous and thus these stars evolve in the direction of the helium-rich homogeneous sequence in the HRD, *i.e* in the blue part of the HR diagram.

Various properties of the present stellar models are indicated in Table 1. Comparing the outputs of the stellar models obtained with different RSG mass-loss rates, one deduces the following points:

- The core He-burning lifetimes are little affected by a change of the RSG mass-loss rates. This comes from the fact that the stellar winds are never strong enough to modify significantly the He-core masses.
- The RSG lifetimes are strongly affected by a change of the RSG mass-loss rates. This can be seen also in the upper panel of Fig. 3. We see that when the red supergiant mass-loss rate increases, the duration of the red supergiant lifetime increases for the 9 $M_\odot$ (by a factor 2 when the mass-loss rate is increased by a factor 10 with respect to the standard value), as the result of the blue loop disappearance. In contrast, the RSG lifetimes decrease for the 20 $M_\odot$ model computed with enhanced RSG mass-loss rates: by a factor 4 for the same change of the mass-loss rates as for the 9 $M_\odot$ model. This comes from the fact that the 20 $M_\odot$ models evolve back to the blue part of the HR diagram when they undergo strong mass-losses (see also Salasnich et al. 1999; Vanbeveren et al. 2007; Yoon & Cantiello 2010; Georgy 2012; Groh et al. 2013a,b). Still increasing the mass-loss rates, the duration of the red supergiant phase for the 9 $M_\odot$ does no longer much change, while for the 20 $M_\odot$, it continues to decrease, by about a factor 2.5 passing from 10 × to 25 × the standard mass-loss rate.
- The lower panel of Fig. 3 shows the fraction of the initial mass which is lost by stellar winds during the RSG phase when various mass-loss prescriptions are used. Let us first comment the 15 $M_\odot$ models. We see that with the standard mass-loss rate, 10-20% (depending on rotation) is lost during the RSG phase. When the mass-loss rates are increased by

Table 1. Core He-burning lifetimes, red supergiant lifetimes, time-averaged mass-loss rates during the red supergiant phase as well as different properties of the last computed models. The abundances are in mass fractions. The metallicity is solar.

$M_{\rm ini}$ $M_\odot$	$\dot{M}$	$t_{\rm He}$ Myr	$t_{\rm RSG}$ Myr	$<\dot{M}>_{\rm RSG}$ $M_\odot\ yr^{-1}$	$M_{\rm fin}$ $M_\odot$	Log $L/L_\odot$	Log $(T_{\rm eff}/K)$	$H_{\rm surf}$	$He_{\rm surf}$	$N/C_{\rm surf}$	$N/O_{\rm surf}$
					$\upsilon_{\rm ini}$=0.						
9	$1\times\dot{M}_{\rm stan.}$	3.6693	1.90	8.66e-08	8.7651	4.5955	3.5416	0.6064	0.3788	1.76	0.67
15	$1\times\dot{M}_{\rm stan.}$	1.3344	1.01	1.50e-06	13.1739	4.7964	3.5592	0.6763	0.3096	2.25	0.56
20	$1\times\dot{M}_{\rm stan.}$	0.8921	0.55	1.62e-05	8.6347	5.1823	3.5730	0.4755	0.5106	86.25	4.31
25	$1\times\dot{M}_{\rm stan.}$	0.7035	0.30	1.34e-05	8.2893	5.3790	4.4332	0.1558	0.8305	117.14	74.55
9	$10\times\dot{M}_{\rm stan.}$	3.5306	3.56	6.49e-07	6.6876	4.0496	3.5685	0.7033	0.2826	1.57	0.42
15	$10\times\dot{M}_{\rm stan.}$	1.4212	0.70	1.32e-05	4.8563	4.7789	3.6116	0.4409	0.5453	118.33	5.07
20	$10\times\dot{M}_{\rm stan.}$	0.8872	0.18	5.00e-05	6.6413	5.0392	3.6257	0.4653	0.5209	236.67	5.07
25	$10\times\dot{M}_{\rm stan.}$	0.6791	0.05	1.30e-04	8.2648	5.2209	4.2322	0.4469	0.5393	185.00	7.40
9	$25\times\dot{M}_{\rm stan.}$	3.4566	3.50	1.58e-06	3.4715	4.0474	3.5448	0.7033	0.2826	1.57	0.42
15	$25\times\dot{M}_{\rm stan.}$	1.4056	0.29	3.04e-05	4.6011	4.7867	3.7388	0.4409	0.5453	118.33	5.07
20	$25\times\dot{M}_{\rm stan.}$	0.8798	0.07	1.27e-04	6.5014	5.0268	3.9331	0.4652	0.5210	236.67	5.07
25	$25\times\dot{M}_{\rm stan.}$	0.6867	0.01	2.56e-04	8.2843	5.2606	4.2330	0.4180	0.5683	130.00	13.45
					$\upsilon_{\rm ini}$=0.4$\upsilon_{\rm crit}$						
9	$1\times\dot{M}_{\rm stan.}$	3.8474	2.30	1.78e-07	8.5175	4.6309	3.5476	0.6487	0.3372	6.33	0.86
15	$1\times\dot{M}_{\rm stan.}$	1.3314	1.19	2.56e-06	11.5156	4.9588	3.5598	0.5951	0.3908	7.00	1.11
20	$1\times\dot{M}_{\rm stan.}$	0.8616	0.34	2.54e-05	7.1785	5.2811	4.3087	0.2381	0.7482	130.00	15.92
25	$1\times\dot{M}_{\rm stan.}$	0.6276	0.13	7.17e-05	9.6896	5.5032	4.3914	0.5120	0.9259	101.87	25.08
9	$10\times\dot{M}_{\rm stan.}$	3.4742	3.49	8.25e-07	6.1108	4.0500	3.5726	0.6539	0.3320	5.64	0.83
15	$10\times\dot{M}_{\rm stan.}$	1.4133	0.43	1.96e-05	5.3064	4.9444	3.6754	0.3916	0.5945	81.25	3.10
20	$10\times\dot{M}_{\rm stan.}$	0.8539	0.11	8.70e-05	7.2971	5.1810	4.2195	0.3780	0.6081	170.00	4.00
25	$10\times\dot{M}_{\rm stan.}$	0.6150	0.03	1.95e-04	9.7153	5.3717	4.5014	0.3186	0.6676	182.50	6.64
9	$25\times\dot{M}_{\rm stan.}$	3.3787	3.15	1.93e-06	2.5951	4.0575	3.6062	0.6524	0.3325	5.70	0.83
15	$25\times\dot{M}_{\rm stan.}$	1.2443	0.19	4.57e-05	5.3091	4.9288	3.6213	0.3891	0.5970	64.00	3.05
20	$25\times\dot{M}_{\rm stan.}$	0.8542	0.04	2.37e-04	7.1887	5.1786	4.2109	0.3755	0.6106	170.00	4.00
25	$25\times\dot{M}_{\rm stan.}$	0.6207	0.01	4.45e-04	9.6199	5.3559	4.5549	0.3298	0.6564	179.49	5.00

an order of magnitude, the fraction increases up to 55-60%. Increasing the mass-loss rates further (from 10x to 25x) does not change this fraction further. This saturation of the mass lost comes from the fact that a star leaves the RSG region when the envelope mass is reduced to a certain value for a given core mass. As a consequence, an increase of the mass-loss rate reduces the time spent in the RSG phase but not the total mass lost. The total mass lost during the RSG phase remains around 40% in the case of the 20 $M_\odot$ stellar model and below 30% for the 25 $M_\odot$ stellar model. *So for stars with initial masses between 15 and 25 $M_\odot$, a blue ward evolution implies the loss of a relatively well fixed amount of mass*. The mass lost is not sufficient for producing a WC star or said in other words a naked CO core (WC are Wolf-Rayet stars characterized by strong carbon and oxygen emission lines). Some mass can be lost after the RSG stage, but this amount is quite modest assuming only quiescent winds. Since the stars become Luminous Blue Variabes (LBVs) when they come back to the blue after losing significant amounts of mass as a RSG (Groh et al. 2013a), additional mass could be lost in LBV eruptions, but the total mass lost is unclear. So already at that stage, one can give an answer to one of the question raised in the introduction: Can such a bluewards evolution (induced by an enhanced RSG mass-loss rate) explain the low luminosity WC stars (Georgy et al. 2012)? The answer seems to be no, confirming the results from Georgy (2012). This conclusion remains valid in case the mass-loss would be due to a mass transfer episode to a binary partner in a close multiple system during the red supergiant phase rather than to an increase of the mass-loss rate as computed here. It is interesting here to mention also the results by Chieffi & Limongi (2013) who obtained for the 20 $M_\odot$ an evolution back to the blue after a RSG phase. The mass loss rates used by these authors somewhat differ from the standard one used in the present model. Their 20 $M_\odot$ enters the WR phase but never becomes a WC star somewhat supporting the present conclusion.

– In general, including the effects of rotation does not change much the results. For a given initial mass, it lowers the RSG lifetimes, while it does not much affect the total mass lost during the RSG phase. This is due to the fact that, when the effects of rotation are included, for a given initial mass, the

RSG is more luminous, thus the mass-losses are stronger. As explained above, this shortens the RSG lifetimes.

4. Properties of red supergiants

Figure 4 shows the location of the Galactic RSGs observed by Levesque et al. (2005) together with the evolutionary tracks computed with and without rotation and for different RSG mass-loss rates. We see that changing the RSG mass-loss rate has no strong impact on the effective temperatures of RSGs, but it modifies the range of luminosities covered by a given initial mass when it is a RSG. The models with an enhanced RSG mass-loss rate encompass a smaller range of luminosities during the RSG phase than those with standard mass-loss rate (compare for instance the RSG part of the tracks for the 15 $M_\odot$ models). This is caused by the much shorter lifetimes spent in the RSG phase for the enhanced mass-loss rate models. The use of tracks computed with different RSG mass loss rate to determine the range of initial masses of an observed RSG, provide somewhat different values. To give a numerical example, if we observe a red supergiant with a luminosity equal to Log $L/L_\odot$ = 5.0, the standard mass loss rate can produce such a red supergiant starting for instance from a 15 $M_\odot$ model, while the 10 × and 25 × models require a higher initial mass, around 18-19 $M_\odot$.

The changes of RSG lifetimes shown in Fig. 3 may have an observable impact on the luminosity function of RSGs in regions of constant star-formation rate[3]. To assess in a quantitative way, a population synthesis model is needed. This will be done in a future work. At the moment, we may already have an idea of the importance of the effect using a more simple approach. In the left panel of Fig. 5, we have plotted the times spent in the RSG stage for our different initial mass models weighted by the Salpeter's initial mass function. We use the quantities for the 9 $M_\odot$ as normalization. More precisely, the vertical axis of the left panel of Fig. 5 indicates $\lg(t_{\rm RSG}(M_{\rm ini})/t_{\rm RSG}(9M_\odot)\times M_{\rm ini}^{-2.35}/9^{-2.35})$, where $t_{\rm RSG}(M_{\rm ini})$ is the RSG lifetime of a stellar model with an initial mass $M_{\rm ini}$. To each initial mass we have attributed a time-averaged luminosity during the RSG phase as it can be deduced from the evolutionary tracks (these average luminosities are log $L/L_\odot \approx$ 3.9, 4.7, 5.0 and 5.3 for respectively the 9, 15, 20 and 25 $M_\odot$). We see that when the RSG mass-loss rate increases, the slope of this "luminosity function" becomes steeper. When the luminosity increases from Log $L/L_\odot$ equal 4 to 5, the number of star decreases by a factor 30 when standard mass-loss rates are used, while it decreases by a factor 500 when models with 25 × the standard mass-loss rate are used. From the left panel of Fig. 5, one deduces that the impact of a change of mass-loss is much stronger than the impact due to rotation (at least for the ranges of values explored here).

To use such a feature to constrain the stellar models, a few conditions must be fulfilled: 1) it requires some completeness of the sample along the whole RSG sequence; 2) the red supergiants, originating from masses equal or larger than 9 $M_\odot$ should be distinguished from luminous AGB stars; 3) the star formation rate should have been constant in the last 30 million years or so. In case these conditions are fulfilled then, the use of the RSG luminosity function to constrain the models has two interesting advantages : 1) it is based on a very simple observations (number ratios); 2) this quantity will provide some constraint on the averaged mass-loss during the RSG phase which is a more useful quantity than the instantaneous mass-loss rate which actually might not be the one responsible for the loss of most of the material during that phase.

[3] In coeval stellar populations, the range of masses of stars, which at a given age, are red supergiants is likely too small, to allow such an effect to be visible.

4.1. Effective temperatures and radii of RSG

The effective temperature or the radius of a RSG is not a very strong prediction of the stellar models since it depends on the choice of the mixing length used to compute the non-adiabatic convection in the envelope. Also the modeling of the convection may be complicated by the fact that the velocity of the convective cells may approach or even supersedes the sound speed implying shocks (see e.g. Maeder 2009). All the present models assume a mixing length, 1.6 times the pressure scale height (see Section 2, note that in these models we did not use a mixing length proportional to the density scale height as for instance was done in Maeder & Meynet 1987). The value 1.6 is calibrated on the Sun. It happens that this mixing length value provides also a good match of the observed positions of the red giant and supergiant branch (see Fig. 2 in Ekström et al. 2012, and Fig. 4).

The radii of the present stellar models during the RSG phase are plotted as a function of the luminosity in the right panel Fig. 5. We see that the radii of the models span a large range of values going from 100 up to 1570 $R_\odot$. During the RSG phase, the variation of the radii for a given initial mass can be quite large for the 9 and 15 $M_\odot$ (factor 6 for the 9 $M_\odot$ and factor 2 for the 15 $M_\odot$). The range of radii covered by the more massive models is much smaller (5-20%). At a fixed luminosity, the range of possible radii for the RSG remains modest. Typically, the shaded area in the right panel of Fig. 5 has a width of 50-100 $R_\odot$.

In the radius-luminosity plane, rotation pushes the tracks of a given mass at higher luminosities but along the same general sequence as the one described by the non-rotating models. Enhancing the mass-loss rates during the RSG phase produces very small effects in general in this diagram. It shifts somewhat the tracks to slightly lower luminosities but again along the same general trend defined by the standard models. There is one exception however in the case of the rotating 15 $M_\odot$ with 25 times the standard mass-loss rates. This model extends much below the general trend. This comes from the fact that the luminosity during the RSG phase decreases a lot for this model as a result of the mass-losses.

When comparisons are made with observed values (see the right panel of Fig. 5), we note a good agreement between models and observations for luminosities between 3.9 up to 5.1-5.2. For higher luminosities, the radii given by the models are too small by about 10-20% with respect to the observations. On this plot some interferometric determinations are also indicated and are also larger than the predicted values. A possibility on the side of the theoretical models to improve the situation, namely to produce larger radii at higher luminosities, would be to decrease the mixing length in the upper luminosity range. It might be also that the values inferred from the observations are slightly too high. The radii of red supergiants is not an easy quantity to measure, since these stars have a very extended and tenuous atmosphere. One can thus easily understand that, depending on wavelength, the radius may differ from the way the radius is determined in our stellar models. Moreover in case the wind is strong enough, it can be optically thick. In that case the surface is no longer observable and a pseudo photosphere at larger radius appears!

Some authors find that the observed radii of RSGs are smaller than those presented in the right panel of Fig. 5. The arguments come from two different approaches: 1) Davies et al. (2013) recently redetermined the effective temperatures of RSGs

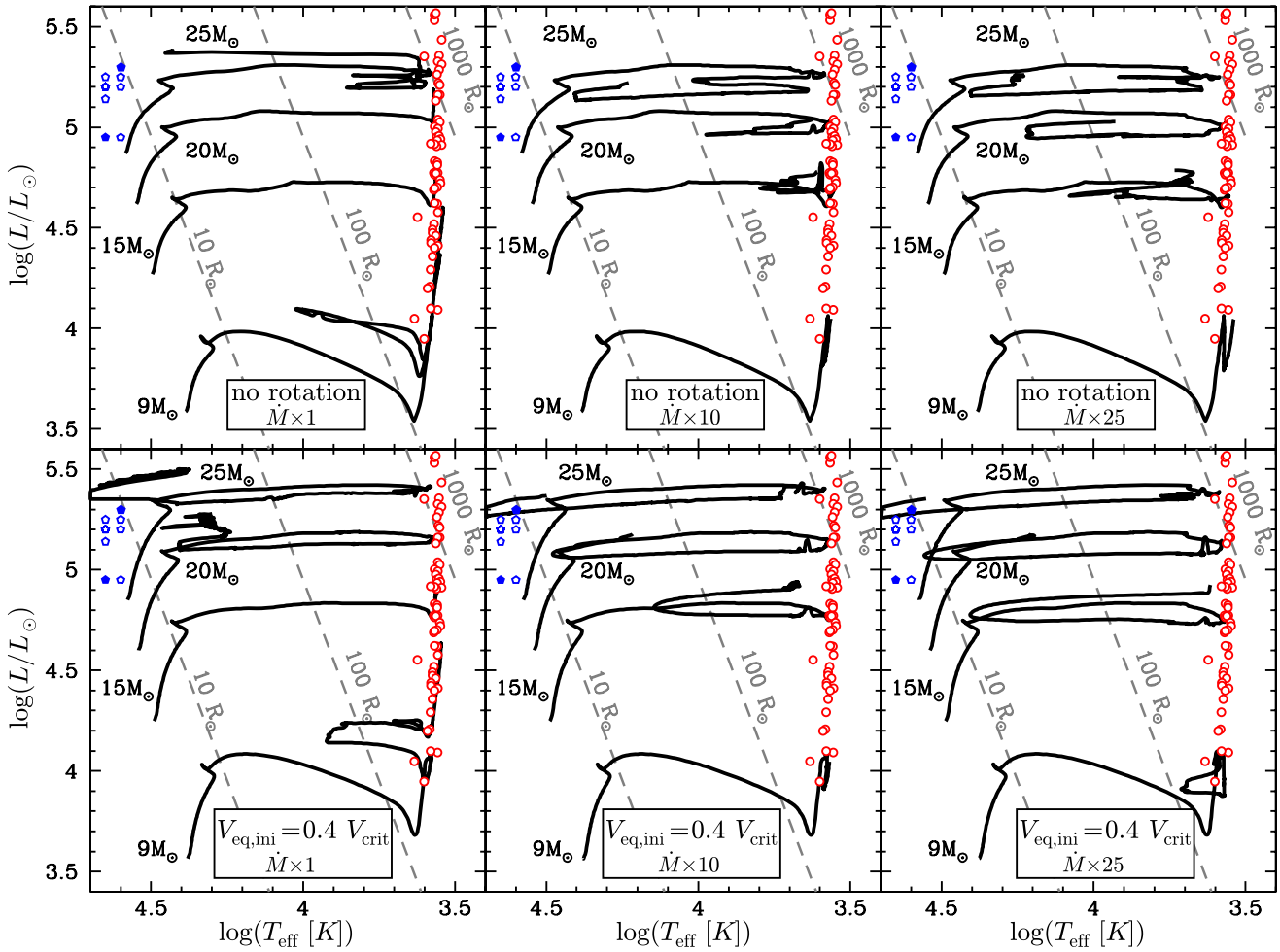

Fig. 4. Evolutionary tracks of models with different initial velocities (non rotating on the top, rotating on the bottom) with different RSG mass-loss rates (increasing from left to right). The (red) empty circles are the positions of the galactic red supergiants observed by Levesque et al. (2005). The blue pentagons are the positions of WC stars as observed by Sander et al. (2012).

in the Magellanic Clouds finding warmer temperatures than found by Levesque et al. (2006) and thus favoring radii of red supergiants about 20-30% more compact. This affects all radii in the whole range of luminosities. The metallicity however is different than solar, therefore we can wonder whether applying their techniques on solar metallicity RSGs, these authors would obtain a similar systematic difference. We note that the Levesque et al. (2006) effective temperatures of Galactic RSGs agree very well with results obtained quite independently by interferometric techniques (see Table 2 in van Belle et al. 2009). 2) Another indirect argument pointing towards smaller radii for red supergiants is the one by Dessart et al. (2013) who argued, based on properties of the type II-P supernova light curve that the progenitors should have a much more smaller radius than commonly assumed (note that this constraint applies to RSG which are the end point of the evolution of the considered star and not to RSGs in general). More precisely, Dessart et al. (2013) show that light curves arising from the explosion of more compact RSG have less blue and shorter plateaus in better agreement with the observation. Typically, these authors show that their 15 $M_\odot$ model with a radius of 500 $R_\odot$ much better reproduces the light curves observed in different filters for the type II-P SN 1999em. Looking at the right panel of Fig. 5, one sees that the 15$M_\odot$ model ends with radii between 300 and 800 $R_\odot$ depending on the RSG mass-loss rate used. In order to obtain, at the end of the evolution, a radius of 500 $R_\odot$, an enhancement factor of the mass-loss rate during the RSG phase between 10 and 25 should be used. Note however, that this is not the only way to obtain a more compact radius. Another solution would be to change the way to compute the outer convective zone (Maeder & Meynet 1987; Dessart et al. 2013).

The above discussion indicates that the radii (or effective temperatures) of RSGs are still in doubt. At the moment, we conclude that the mixing length considered in the present models do in general a good job. An enhanced RSG mass-loss rate can explain some more compact radii for RSGs at the pre-supernova stage, in the mass range around 15 $M_\odot$.

4.2. The surface composition

Figure 6 shows how various abundance ratios evolve during the red supergiant phase for different initial masses, rotations and RSG mass-loss rates. The non-rotating tracks enter into the RSG with N/C, N/O and $^{12}C/^{13}C$ ratios which are equal to the initial values (that means that the tracks begin at the ordinate 0 in the two upper panels, at the coordinate (0,0) in the lower left panel and at the ordinate around 90, well outside the range of values shown in the lower right panel). Then the tracks go up (increases of nitrogen and decreases of carbon and oxygen), except in the

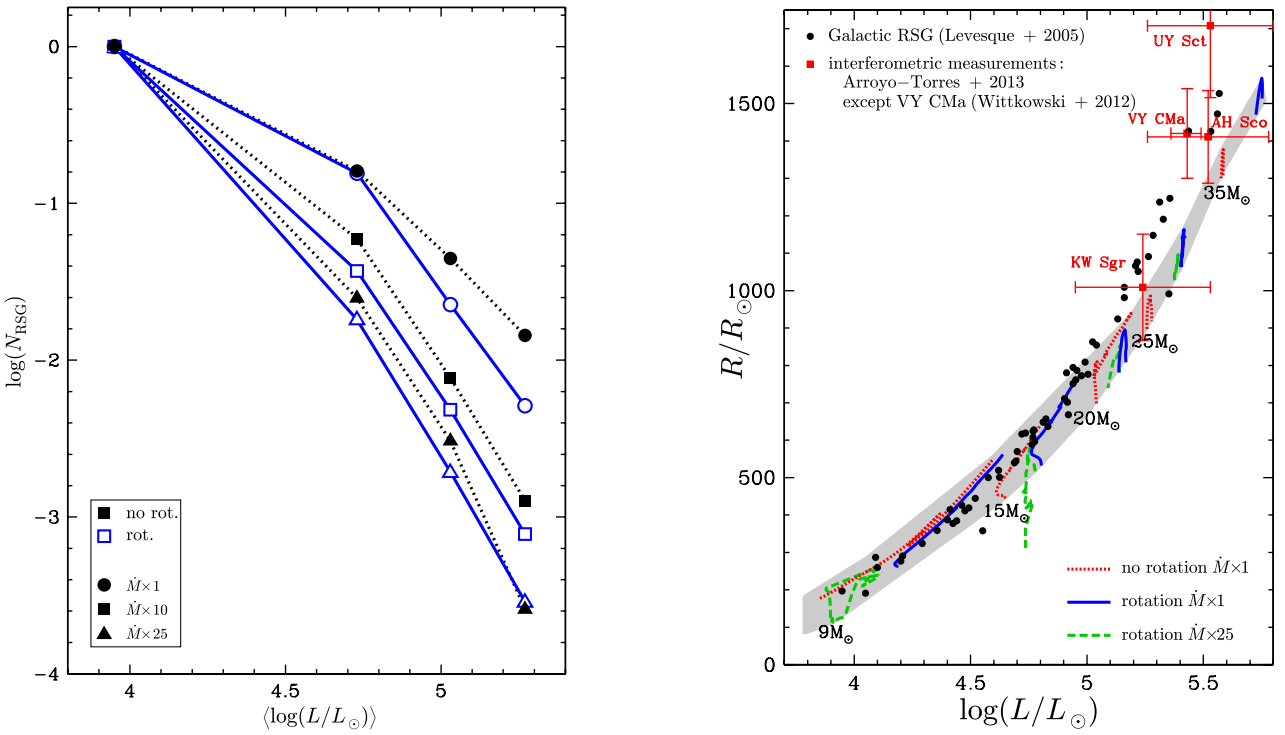

Fig. 5. *Left panel:* Number of red supergiants as a function of luminosity in a constant star formation rate region (see text). Numbers are normalized to the 9 $M_\odot$. Dots indicate the values obtained for the 9, 15, 20 and 25 $M_\odot$ models from left to right. *Right panel:* Radii of various stellar models during the RSG phase (Log T_{eff} < 3.6) as a function of the luminosity. The shaded area covers the region covered by the models with different initial masses, rotations and mass-loss rates. The 25 times enhanced, rotating 15 $M_\odot$ is the only model which evolves out of this region. The initial mass is indicated at the minimum luminosity predicted by the models for this mass.

case of the lower right panel where the tracks go down when time increases ($^{12}C/^{13}C$ decreases).

Let us first focus on the case of the non-rotating 20 $M_\odot$ with standard mass-loss. We see that the RSG tracks cover a very large range of surface abundances, while the luminosity does not vary much. The change of the surface abundances comes from the deepening of the outer convective zone that dredges-up some nuclearly processed material at the surface. For the N/C and N/O ratios, the changes are gradual and the different ratios are relatively well distributed along the time sequence. For the $^{12}C/^{13}C$ ratio, the decrease is quite rapid and most of the time the model will show values below about 20. This is due to the fact that the $^{12}C/^{13}C$ ratio is significantly decreased on a greater extent of the mass of the star than the N/C or the N/O ratio.

When the mass-loss rate is increased during the RSG phase, no significant differences appear for the 20 $M_\odot$ model. However, due to the reduction of the RSG lifetime when the mass-loss rates are larger, the ranges of surface abundance values are slightly more restricted. The same occurs for the luminosity.

When, for the 20$M_\odot$ model, rotational mixing is accounted for (continuous lines), we notice two significant differences with respect to the non-rotating cases. First, at the entrance of the RSG phase, the N/C, N/O and $^{12}C/^{13}C$ ratios are already reflecting the presence of nuclearly processed material at the surface. Second, the ranges of surface abundance ratios covered during the RSG phase are much smaller. This comes from the fact that the outer convective zone in the rotating model does not extend as deep as in the non-rotating one, because in rotating models, helium cores are larger than in the non-rotating ones. As a consequence, the H-burning shell, which acts as a barrier for the deepening of the convective envelope, is at a larger lagrangian mass coordinate in the rotating models.

Similar qualitative behaviors as for the 20 $M_\odot$ model are obtained for the 25 $M_\odot$ models. In the case of the 15 $M_\odot$ model, we just note that when the RSG mass-loss rate increases, then a larger range of abundance ratios are obtained during the RSG phase for the N/C and N/O ratios. This comes from the fact that in the case of the 15 $M_\odot$ model, the mass lost during the RSG increases a lot when one passes from the standard to the enhanced RSG mass-losses (see also Fig. 3). The 9 $M_\odot$ appears in Fig. 6 just through the standard mass-loss rate models (the part of the track shown corresponds to the evolution back to the red after a blue loop.). The enhanced mass-loss rate models are at too low luminosities to show up on this plot.

The lower left plot shows the track in the N/C versus N/O plane. We see that whatever the model considered the tracks are very similar. As discussed by Przybilla et al. (2010) and Maeder et al. (2014), this results from the fact that the tracks in this plane are more reflecting the CNO cycle itself than the details of the stellar models.

Recently surface abundances for three red supergiants belonging to the cluster RSGC2 have been obtained using the NIR spectrograph GIANO on Telescopio Nazionale Galileo (TNG) by Origlia et al. (2013). The positions of these stars are indicated in Fig. 6. RSGC2 is a young massive cluster (40 000 $M_\odot$) at a distance of about 3.5 kpc from the Galactic center (Davies et al. 2007). This analysis finds that the [C/Fe] ratio is depleted by a factor between two and three confirming the result by Davies et al. (2009). They also find that the $^{12}C/^{13}C$ ratio is low (between 9 and 11). Values for the N/C and N/O values are also indicated for Betelgeuse and IRS 7 (Lambert et al. 1984; Carr et al. 2000). The $^{12}C/^{13}C$ ratios are indicated for alpha Sco (Hinkle et al. 1976) and VY CMa (Matsuura et al. 2014).

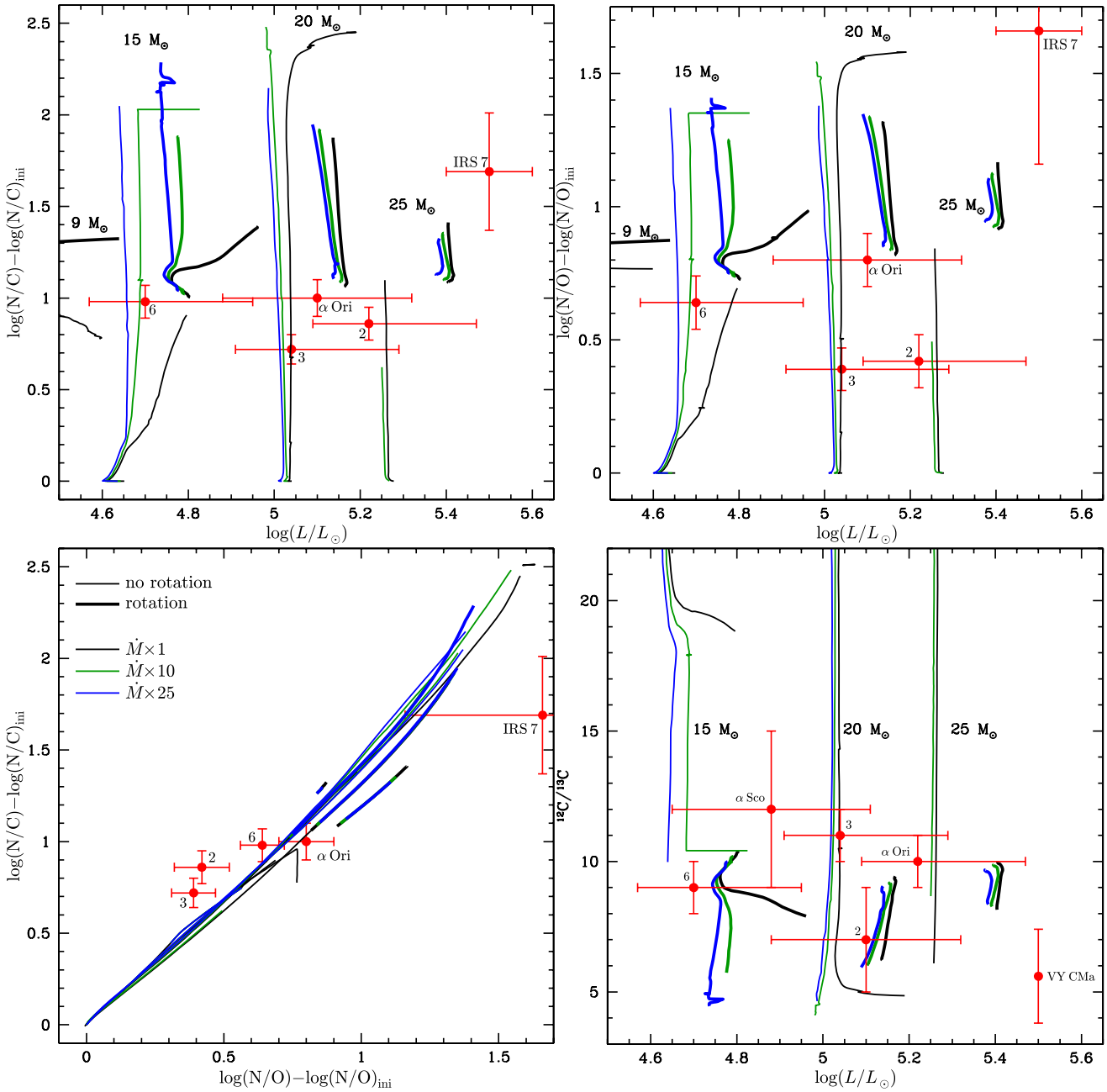

Fig. 6. *Upper left panel:* Surface N/C ratios during the red supergiant phase normalized to the initial one in logarithm and in mass fraction as a function of the luminosity for various models. The red full dots are for observed values, stars labeled 2, 3 and 6 are taken from Origlia et al. (2013), α Ori from Lambert et al. (1984) and IRS 7 from Carr et al. (2000). *Upper right panel:* Same as Upper left panel but for the N/O surface abundance ratio. *Lower left panel:* Tracks during the red supergiant phase in the N/C versus N/O plane (surface values). The models are the same as in the upper left figure. *Lower right panel:* Surface ^{12}C/^{13}C ratios for the same models as in the upper left figure. The dots are observed values for 6, α Sco (Hinkle et al. 1976), 3, 2, alpha Ori and VY CMa (Matsuura et al. 2014).

For the N/C and N/O ratios, with the exception of IRS 7, the ratios may be reproduced by the non-rotating models (whatever the mass-loss rate during the RSG stage) or by models with an initial rotation smaller than the one corresponding to $\upsilon_{\rm ini}/\upsilon_{\rm crit}$ 0.4. The case of IRS 7, a star belonging to the galactic centre, does appear difficult to be explained by the present models. It is also quite off from the predicted relations in the N/C versus N/O plane. The initial abundance ratios in the galactic centre may be different from solar ones, this might explain part of these differences.

We see that the observed ^{12}C/^{13}C ratios are all very small and appear slightly more compatible with models having undergone some mixing before entering the RSG stage. This is in line with the conclusions by Davies et al. (2009) and Origlia et al. (2013), and this conclusion is not changed considering modifications of the RSG mass-loss rates. Actually we see that the surface abundances are much more sensitive to rotation than to the mass-loss rates during the RSG phase. We can thus conclude that the constraints on the surface abundances of red supergiants cannot be used to discard any of the models presented here, even those computed with the most extreme mass-loss rates during the RSG phase.

Table 2. Properties of RSGs identified as SN progenitors. All these supernovae are of type II-P.

SN	[O/H]	Log L/L$_\odot$	Log ($T_{\rm eff}/K$)	Reference
2003gd	8.4	4.3±0.3	3.55	Smartt (2009)
2004A	8.3	4.5±0.25	3.55	Smartt (2009)
2004et	8.3-8.9	4.8	3.56	Fraser et al. (in prep.)
2005cs	8.7	4.25±0.25	3.55	Smartt (2009)
2008bk	8.4-8.7	4.84±0.12	3.64	Maund et al. (2014)
	8.5	4.57±0.06	3.56±0.006	Van Dyk et al. (2012b)
2009md	8.96±0.04	4.54 ±0.19	3.55±0.010	Fraser et al. (2011)
2012A	8.12±0.08	4.73±0.14	3.58±0.050	Tomasella et al. (2013)
2012aw	8.6±0.2	5.3±0.3	3.60±0.050	Fraser et al. (2012)
	8.7	5.21±0.03	3.56±0.025	Van Dyk et al. (2012a)
2013ej	-	4.65±0.20	3.57±0.035	Fraser et al. (2014)

4.3. Surface and interior rotation of red supergiants

During the RSG phase, the surface velocities at the equator are in general below 1 km s^{-1}. Surface velocities as low as 0.1 km s^{-1} or even a few 0.01 km s^{-1} can be reached. Models with enhanced mass-loss during the RSG phase present not significantly different surface velocities with respect to the standard mass-loss rate case.

The deprojected surface rotation velocity of Betelgeuse is about 15 km s^{-1} (Uitenbroek et al. 1998), so significantly above the values obtained by the present models, but still well below the typical critical velocity (between 40-60 km s^{-1}). It is interesting to note that Betelgeuse is among the few red supergiants that are runaway stars. Runaway stars move supersonically through the interstellar medium (Blaauw 1961). Such high speed may be acquired through few-body dynamical encounter (Poveda et al. 1967), or binary-supernova explosions (Blaauw 1961; Stone 1991). The supersonic movement produces an arc-like shape bow shock that can be detected at many wavelengths from infrared to X-ray wavebands. As written by Gvaramadze et al. (2014), most of bow-shock producing stars are either on the main-sequence or are blue supergiants, while there are no Wolf-Rayet stars and only three among RSG: Betelgeuse (Noriega-Crespo et al. 1997), μ Cep (Cox et al. 2012) and IRC-10414 (Gvaramadze et al. 2014). Is the fast surface rotation observed for Betelgeuse related to the process which made it a runaway stars? We leave that question open.

The ratio between the angular velocity of the core and of the surface is very large, being in the range of 10^5-10^9 for most models. Enhanced mass-loss rate models in general restrict these ratios to values below 10^7. Let us recall here that the present models do not account for any additional transport mechanism in addition to those associated to shear turbulence and meridional currents. Asteroseismological analysis of red giants indicates that some additional transport mechanism is at work in stars with masses around 1 M$_\odot$ (Beck et al. 2012; Eggenberger et al. 2012; Marques et al. 2013). This additional mechanism produces stronger coupling between the core and envelope, reducing the ratio between the core and envelope rotation. It would be very interesting to obtain for red supergiants similar constraints.

4.4. Type II supernovae with a red supergiant progenitor

In Table 2, we list some properties of the RSGs identified as SN II-P progenitors according to the most recent determinations in the literature. Only those progenitors of type II-P supernovae for which the luminosity is available are indicated, letting aside those for which only an upper limit is given. Note that when no effective temperature is given, an arbitrary value of 3.55 is attributed to the progenitor, based on the fact that according to the references quoted, the progenitor was likely a red supergiant. The metallicities given are very indicative.

Table 3. Durations of various post-MS stages in Myr.

$M_{\rm ini}$	t_{B1}	t_{Y1}	t_{RSG}	t_{Y2}	t_{B2}	t_{WR}	t_{pRSG}	t_{pMS}
				$v_{\rm ini}$=0.				
				1×$\dot{M}_{\rm stan.}$				
15	0.210	0.150	1.008	0	0	0	0	1.580
20	0.271	0.092	0.549	0	0	0	0	0.912
25	0.100	0.088	0.296	0.233	0	0.001	0.234	0.718
				10×$\dot{M}_{\rm stan.}$				
15	0.210	0.150	0.703	0.393	0	0	0.393	1.456
20	0.271	0.092	0.187	0.357	0	0	0.357	0.907
25	0.100	0.087	0.052	0.093	0.361	0	0.454	0.694
				25×$\dot{M}_{\rm stan.}$				
15	0.210	0.150	0.293	0.502	0.286	0	0.788	1.440
20	0.271	0.092	0.074	0.194	0.269	0	0.463	0.900
25	0.100	0.103	0.012	0.248	0.238	0	0.486	0.701
				$v_{\rm ini}$=0.4$v_{\rm crit}$				
				1×$\dot{M}_{\rm stan.}$				
15	0.060	0.110	1.193	0	0	0	0	1.363
20	0.051	0.157	0.345	0.056	0.271	0	0.326	0.880
25	0.014	0.003	0.130	0.080	0.415	0	0.495	0.641
				10×$\dot{M}_{\rm stan.}$				
15	0.060	0.108	0.430	0.729	0.117	0	0.847	1.445
20	0.051	0.157	0.111	0.037	0.516	0	0.553	0.872
25	0.014	0.004	0.033	0.103	0.475	0	0.578	0.632
				25×$\dot{M}_{\rm stan.}$				
15	0.060	0.107	0.193	0.732	0.184	0	0.916	1.276
20	0.051	0.158	0.045	0.036	0.583	0	0.619	0.873
25	0.014	0.004	0.012	0.098	0.506	0	0.604	0.634

Looking at the positions in Figs. 7 of these nine progenitors, we can make the following comments:

- Most of the progenitors have Log $L/L_\odot$ between 4.2 and 4.8, which means well within the luminosity range of stellar models ending their lifetimes as red supergiants when standard mass-loss rates are used. This holds for both rotating and non-rotating models. Models with the mass-loss rate increased by a factor of 10 can barely match the observed RSG at the pre-SN stage, meaning that we cannot rule out that models with modest mass-loss enhancements $\dot{M}$ (2–4) would be able to fit the observations. On the other hand, these progenitors cannot be fitted by models with the mass-loss rate enhanced by a factor of 25, which predict too low luminosities or too high effective temperatures in this luminosity range.
- As discussed in Groh et al. (2013b), the initial mass of observed progenitors that are RSGs depend on rotation, with non-rotating models yielding a larger initial mass than rotating models. We refer to their Table 6 for determinations of the initial mass of SN II-P progenitors based on rotating and non-rotating models.
- For SN 2004et, the nebular-phase spectral modeling made by Jerkstrand et al. (2012) constrains the progenitor mass to $M_{\rm ZAMS}$ = 15 M$_\odot$, with a pre-SN oxygen mass of 0.8 M$_\odot$. This oxygen mass is quite consistent with our non-rotating 15 M$_\odot$ model with standard mass-loss rate during the RSG phase, which predicts that an oxygen mass of 0.8 M$_\odot$ would be ejected assuming a remnant mass of about 1 M$_\odot$.
- The case of 2012aw (the most luminous progenitor) could be explained by our non-rotating standard mass-loss rate model for a 20 M$_\odot$ star or from a model with a slightly higher initial

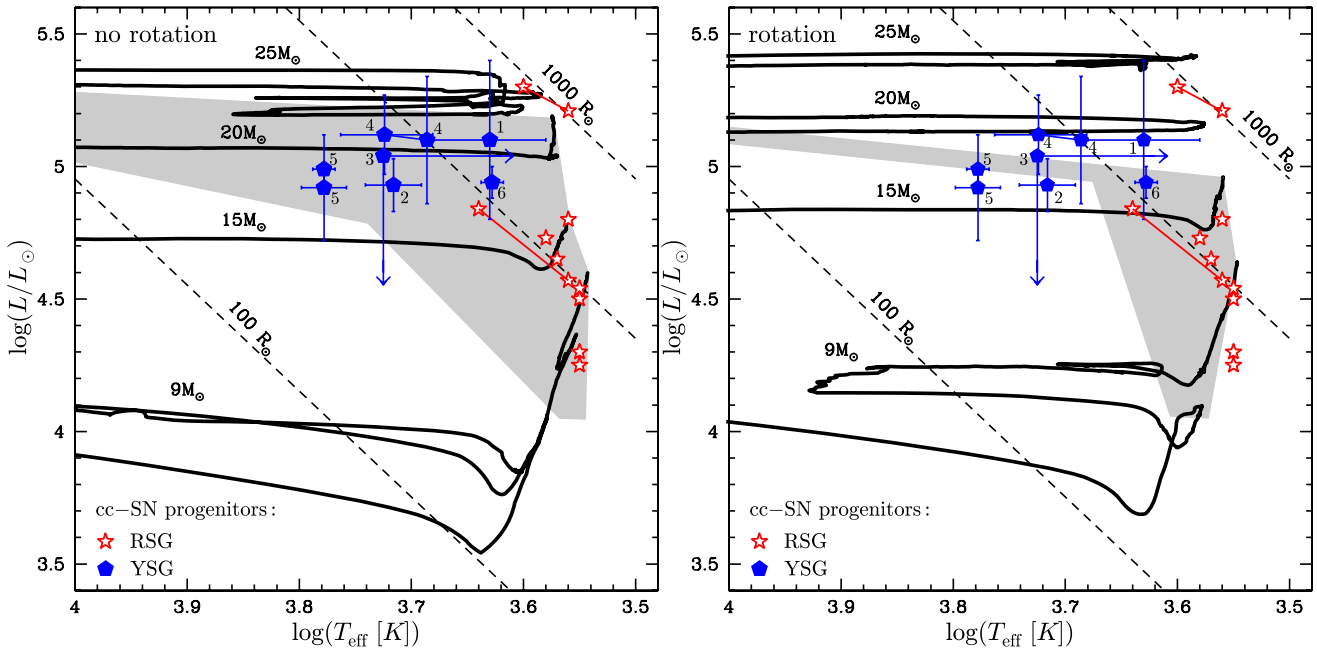

Fig. 7. *Left panel:* Evolutionary tracks in the HR diagram for the non-rotating models and computed with the standard mass-loss rates with superposed the positions of progenitors of core collapse supernovae. Empty stars are for those which are red supergiants (see Table 2), filled pentagons are for those which have a yellow supergiant as progenitors (see Table 6). A continuous segment links positions of the same SN progenitors obtained by various authors. Progenitors of supernovae predicted by the non-rotating models computed with the various RSG mass loss rates are found in the shaded area. Progenitors obtained with standard RSG mass-loss rates occupies the upper part as well as the right part of the shaded region, while the progenitors obtained from enhanced RSG mass-loss rate models are on the lower-left region of the shaded area. Lines of constant radius are indicated, the line intermediate between the 100 and 1000 $R_\odot$ corresponds to a radius of 500 $R_\odot$. *Right panel:* Same as left panel with evolutionary tracks in the HR diagram for the rotating models and computed with the standard mass-loss rates. Progenitors of supernovae predicted by the rotating models computed with the various RSG mass loss rates are found in the shaded area.

mass (although less massive than 25 $M_\odot$). It appears more difficult to fit that progenitor from rotating models with standard mass-losses. Such a highly luminous RSG progenitor cannot be reproduced by enhanced mass-loss rate models, with or without rotation. More generally, the upper luminosity of stars ending their evolution as a red supergiant decreases when the initial rotation and/of the mass-loss rate during the red supergiant stage increases. This can well be seen in Fig. 8.

– For the 9 $M_\odot$ models, an enhancement in the mass-loss rate at the RSG phase decreases the luminosity at the pre-SN stage. This may have interesting consequences for the nature of low-luminosity SN II-P progenitors and the minimum initial mass of stars that produce core-collapse SNe.

From the points above, we conclude that the positions in the HRD of the present RSG supernova progenitors are best described by the standard mass-loss models (see Sect. 8.1 of Groh et al. 2013b), although modest mass-loss rate enhancements (2–4) cannot be discarded.

5. Evolution of post-RSG stars

On Fig. 4, we can see how the post red supergiant tracks change when different RSG mass-loss rates are applied. If we focus on the case of the 20 $M_\odot$ model, we can note that increasing the RSG mass-loss extends the post RSG track towards bluer positions. For the 15 $M_\odot$ model, a qualitatively similar behavior is observed although less marked. In the case of the 25 $M_\odot$, on the other hand, we obtain that the evolution back to the blue, which was already present in the standard mass-loss rate model, is slightly shortened in its extension in effective temperatures and does occur at lower luminosities when enhanced mass-loss rate models are used. For all the cases discussed above (15 to 25 $M_\odot$), the star would explode as an LBV or yellow hypergiant (Groh et al. 2013a,b). Finally, as already explained in Section 3, increasing the RSG mass-loss rate for the 9 $M_\odot$ keeps the star in the red part of the HRD. When rotation is accounted for, these features remain very similar.

Table 3 shows the time spent by the present stellar models in the blue, yellow, red regions of the HR diagram, and as Wolf-Rayet stars. Following the recent results from Groh et al. (2014), we consider the models as being WR stars when $\log(T_{\rm eff}/K) > 4.36$ and the mass fraction of hydrogen at the surface is less than 0.30. We consider the model as being in the blue region of the HR diagram when $\log(T_{\rm eff}/K) > 3.90$ and when it is not a WR star. Our criteria for determining the blue region include blue supergiants, blue hypergiants, and LBVs. We distinguish the time spent in the blue before (t_{B1}) and after the RSG phase (t_{B2}). Yellow stars are those stars with $3.66 < \log(T_{\rm eff}/K) < 3.90$, which encompasses yellow supergiants and yellow hypergiants. Also here, we note t_{Y1}, respectively t_{Y2}, the duration of the yellow phase before and after the RSG phase. Red supergiants are considered as those stars with $\log(T_{\rm eff}/K) < 3.66$ for the initial stellar masses shown in Table 3.

Globally, we see that the total time spent after the Main Sequence phase (see $t_{\rm pMS}$ in Table 3) is not much affected by a change of the RSG mass-loss rate. As already mentioned before, the change of the RSG mass-loss rate has a deep impact on the duration of the post RSG phase (see $t_{\rm pRSG}$ in Table 3). As an example, the 15 $M_\odot$ with standard mass-loss rate spend no time in post RSG phases, while the enhanced mass-loss rate model

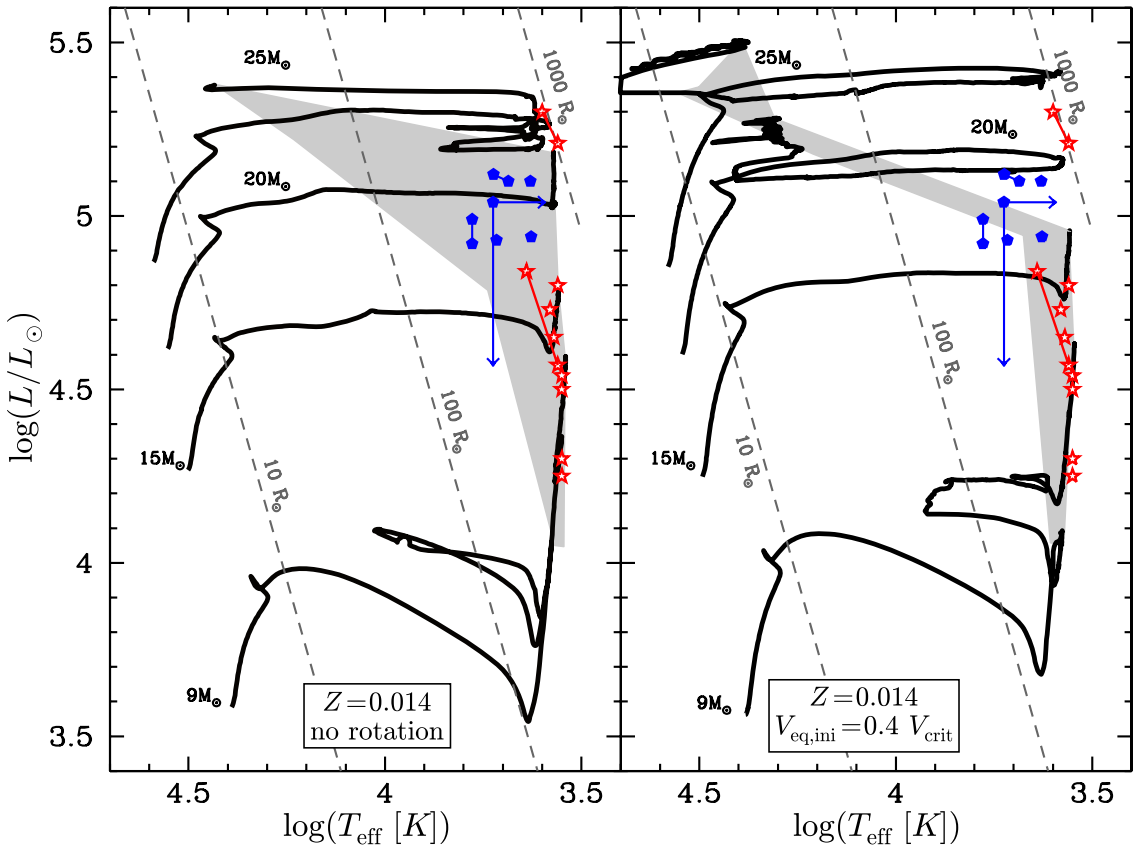

Fig. 8. *Left panel:* Evolutionary tracks in the HR diagram for the non-rotating models and computed with the standard mass-loss rates with superposed observed positions of progenitors of core collapse supernovae. The observed data are the same as in Figs. 7. For purpose of clarity, the error bars are not shown. Progenitors of supernovae predicted by the non-rotating models computed with the various RSG mass loss rates are found in the shaded area. *Right panel:* Same as the left panel for rotating stellar models. The shaded area shows the region where the progenitors of supernovae are found according to the rotating models with various RSG mass loss rate prescriptions.

spends a fraction between 27 and 72% of the whole post MS period.

The fraction of the post MS phase that is spent in the yellow and blue regions depends on the initial mass, rotation and the RSG mass-loss rates. When the stellar model evolves back to the blue, then the duration of the post-RSG yellow or blue supergiant phase is in general larger than the duration of the corresponding phases before the RSG stage. Therefore, when a blue ward evolution occurs, there is a greater chance that a given blue or yellow supergiant be a post RSG object than a pre RSG one.

The enhanced mass-loss models never enter into the WR stage[4]! This might be surprising at first sight since one would have expected that stronger mass-losses during the RSG phase would favor the formation of WR stars. Actually, as noted above, when the mass-loss rate is increased, the duration of the RSG phase is shortened while the total mass lost remains more or less constant. As a consequence the star with enhanced mass-loss rate will expose at the surface more or less the same interior layer but at an earlier stage of its evolution. This explains why the surface composition will reflect a less advanced evolutionary phase. So, increasing the mass-loss rate during the RSG phase, would actually decrease the number of WR stars formed through the single star channel! A caveat concerns the occurrence of eruptions during the post-RSG phase, when the star becomes a yellow hypergiant or an LBV (Groh et al. 2013b), which could remove additional mass from the star and favor the formation of WRs. Therefore, it seems that the key for forming WR stars at low-luminosity from single stars is the post-RSG mass-loss.

5.1. Effective temperatures and characteristics of SN progenitors

In Fig 8, we show the regions in the HR diagrams (see the shaded areas), where the models computed with different RSG mass-loss rates predict the positions of the SNe progenitors[5]. When the RSG mass-loss rate is increased, as also discussed by Georgy (2012), the end point of the evolution is shifted to the blue for the 15 and 20 $M_\odot$ models.

Figure 9 shows the structure of the pre-supernovae models for different initial masses, rotation and prescriptions for the mass-loss rate during the RSG phase. In Table 4, the final radii, masses, masses of the hydrogen-rich envelope[6], the masses of

[4] This of course is dependent on the way we define a WR star but the feature that would remain is the fact that whatever the type of the star, the surface composition of the enhanced RSG mass-loss models correspond in general to less CNO processed material than the surface composition of the standard models.

[5] The models were computed until the end of the core C- or He-burning phase. The positions of the models at the end of the He-burning phase can still evolve during the core carbon burning phase, but in absence of very strong mass-loss outburst, the displacement in the HR diagram remains modest and we shall consider the positions of these models as a good proxy for the pre-supernova positions.

[6] The mass of the hydrogen-rich envelope, $\Delta M_{\rm H}$, is simply the difference between the final mass and M_α. Note that hydrogen can also be present outside $\Delta M_{\rm H}$, in the outer layers of M_α. This is the reason why,

Table 4. Characteristics of the models at the end of the core He- or C-burning phase (models at the end of the C-burning phase are indicated by an asterisk).

M_{ini}	$\dot{M}$	R_{fin}	M_{fin}	ΔM_H	M_α	M_{CO}	M_{rem}	M_{grav}	m_H	m_{He}	m_C	m_O	L	Ω (NS)	P (NS)
$M_\odot$	$M_\odot$ y^{-1}	$R_\odot$	$M_\odot$	$M_\odot$	$M_\odot$	$M_\odot$	$M_\odot$	$M_\odot$	$M_\odot$	$M_\odot$	$M_\odot$	$M_\odot$	10^{49} cm^2 g/sec	10^4 sec^{-1}	10^{-4} sec
							υ_{ini}=0.								
9	1×$\dot{M}_{stan.}$	548	8.765	7.555	1.21	1.20	1.12	1.05	4.58	2.87	0.05	0.07	–	–	–
15	1×$\dot{M}_{stan.}$	637	13.174	8.914	4.26	2.24	1.46	1.33	5.76	4.94	0.37	0.52	–	–	–
20	1×$\dot{M}_{stan.}$	932	8.635	2.425	6.21	4.00	1.91	1.68	1.15	3.31	0.49	1.16	–	–	–
25	1×$\dot{M}_{stan.}$	22	8.289	0.169	8.12	5.95	2.41	2.03	0.03	2.20	1.01	2.28	–	–	–
9	10×$\dot{M}_{stan.}$	258	6.688	4.558	2.13	0.88	0.88	0.84	3.19	2.43	0.10	0.05	–	–	–
15	10×$\dot{M}_{stan.}$	491	4.856	0.616	4.24	2.24	1.46	1.33	0.28	2.01	0.52	0.55	–	–	–
20	10×$\dot{M}_{stan.}$	620	6.641	0.541	6.10	3.81	1.86	1.65	0.27	2.38	0.75	1.30	–	–	–
25	10×$\dot{M}_{stan.}$	47	8.265	0.365	7.90	5.54	2.30	1.96	0.16	2.44	1.06	2.17	–	–	–
9	25×$\dot{M}_{stan.}$	287	3.471	1.361	2.11	0.87	0.87	0.83	0.93	1.55	0.07	0.02	–	–	–
15	25×$\dot{M}_{stan.}$	276	4.601	0.401	4.20	2.21	1.45	1.32	0.21	1.98	0.44	0.53	–	–	–
20	25×$\dot{M}_{stan.}$	148	6.501	0.461	6.04	3.75	1.85	1.64	0.22	2.32	0.76	1.28	–	–	–
25	25×$\dot{M}_{stan.}$	49	8.284	0.264	8.02	5.66	2.33	1.98	0.14	2.41	1.07	2.24	–	–	–
							υ_{ini}=0.4υ_{crit}								
9*	1×$\dot{M}_{stan.}$	555	8.517	5.437	3.08	1.64	1.30	1.20	3.53	3.03	0.18	0.34	6.24	5.18	1.21
15	1×$\dot{M}_{stan.}$	766	11.516	6.506	5.01	2.78	1.60	1.44	3.72	4.62	0.48	0.97	9.50	6.56	0.96
20*	1×$\dot{M}_{stan.}$	35	7.178	0.008	7.17	4.73	2.10	1.82	0.02	1.61	0.87	2.10	11.87	6.52	0.96
25*	1×$\dot{M}_{stan.}$	31	9.690	0.000	9.69	7.09	2.69	2.22	0.00	1.59	1.61	3.60	17.77	7.98	0.79
9	10×$\dot{M}_{stan.}$	254	6.111	3.811	2.30	0.96	0.96	0.91	2.48	2.44	0.11	0.07	4.43	4.84	1.30
15	10×$\dot{M}_{stan.}$	442	5.306	0.386	4.92	2.79	1.60	1.44	0.15	1.89	0.55	1.05	2.96	2.05	3.07
20	10×$\dot{M}_{stan.}$	47	7.297	0.337	6.96	4.86	2.06	1.79	0.15	2.21	0.89	1.93	4.89	2.50	2.51
25	10×$\dot{M}_{stan.}$	16	9.715	0.245	9.47	7.02	2.67	2.21	0.09	2.42	1. 35	3.05	0.38	0.17	36.45
9	25×$\dot{M}_{stan.}$	219	2.595	0.325	2.27	0.94	0.94	0.89	0.21	1.32	0.07	0.04	4.34	4.85	1.29
15	25×$\dot{M}_{stan.}$	557	5.309	0.609	4.70	2.71	1.58	1.43	0.24	2.03	0.61	0.78	7.72	5.39	1.16
20	25×$\dot{M}_{stan.}$	49	7.189	0.299	6.89	4.52	2.04	1.78	0.14	2.17	0.89	1.88	4.79	2.68	2.34
25	25×$\dot{M}_{stan.}$	12	9.620	0.230	9.39	6.88	2.64	2.18	0.86	2.32	1.37	3.03	0.38	0.17	36.37

the helium, carbon-oxygen cores, of the remnants are indicated together with the integrated mass in the envelope of the quantities of hydrogen, helium, carbon and oxygen. For the rotating models, the angular momentum in the remnant, the angular velocity of the neutron star and its period at birth are also provided. For computing these quantities we followed the same method as in Georgy et al. (2012). We can note the following effects of enhancing the mass-loss rate during the RSG phase:

- From table 4, we see that the models with enhanced mass-loss rates during the RSG phase have in general smaller He and CO cores at the end of their evolution, which is of course expected. We note however that due to the interplay between mass-loss and lifetime during the RSG stage, some models may present slightly larger He or even CO cores for higher RSG mass-loss rates (see for instance the case of the rotating 20 $M_\odot$ with 1 and 10 × the standard mass-loss rate). On the whole, however, the effects on the cores remain modest.
- We see also that in the most extreme case of mass-loss during the RSG phase considered here, the final mass of the star contains 30-40% of the initial mass, whatever the initial mass between 9 and 25 $M_\odot$ (see the bottom panels of Fig. 9 and, in these panels, the bottom line framing the "WIND" region).
- One can wonder whether the change of the mass-loss rate during the RSG phase can impact the angular momentum of the core? We see that the angular momentum in the remnant decreases when the RSG mass-loss rate increases. However, the changes are very modest. Even considering the models with a mass-loss increased by a factor 25 would produce extremely rapidly rotating neutron stars. For instance the largest period obtained here for a neutron star would be of 3.6 ms. For comparisons, the observed shortest periods for young pulsars are around 20 ms, thus five time larger than the periods obtained here. So some angular momentum should still be lost, either during the previous phases (Heger et al. 2005) or at the time of the SN explosion (Blondin & Mezzacappa 2007) or during the early phases of the evolution of the new born neutron star.
- The RSG mass-loss increase has the strongest impact on the structure of the envelope in the range of initial masses between 9 and 15 $M_\odot$. We see indeed that very little changes occur for the 25 $M_\odot$, while important changes occur for the 9 or 15 $M_\odot$. This is quite natural since, the 25 $M_\odot$ models spend a very short time into the red supergiant phase anyway, so that changing the mass-loss rates during the short RSG phase will have only a marginal impact. This also justifies the reason why we stopped our investigation to this upper mass limit.
- We see that the H-rich envelope is significantly reduced by the high RSG mass-loss rates. On the other hand, as already noted above, the masses of the He-rich layer and of the CO core are generally only slightly changed.
- Looking at the structure of stars finishing their life as red supergiants (see red stars in the upper part of each panel of Fig. 9), we note that red supergiants can exist for very different masses of the H-rich envelope (see also Groh et al. 2013b). Actually the range for the masses of H-rich envelopes in RSG pre-supernova models can range from more

in some models, the integrated mass of hydrogen, m_H, can be larger than ΔM_H. Here, M_α is defined here as the lagrangian mass coordinate where the mass fraction of helium becomes superior to 75% going from the surface to the center.

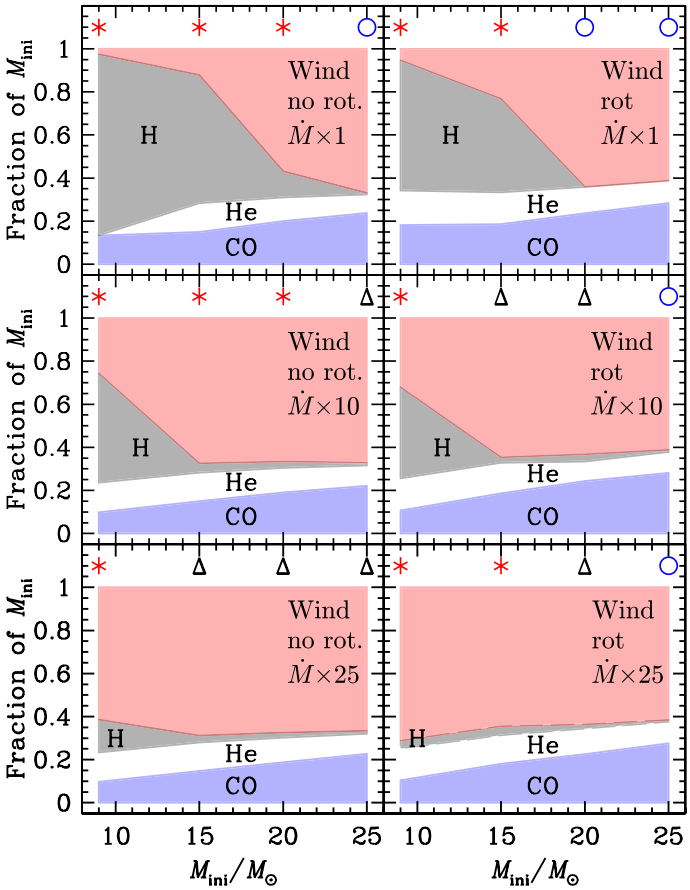

Fig. 9. Fraction of the initial mass of the star ejected by stellar winds during the whole stellar lifetime (red shaded area). The mass in the H-rich envelope, He-rich region and CO core in the pre-supernova model as a function of the initial mass are indicated by the black, white and blue regions. Cases for various mass-loss rates during the RSG phase without and with rotation are shown. The symbols in the upper part of each panel indicate the range of effective temperatures of the model at the pre-supernova stage: log T_{eff} inferior to 3.65 are indicated by (red) stars, log T_{eff} between 3.65 and 4.30 by (black) triangles and log T_{eff} greater than 4.3 by (blue) circles.

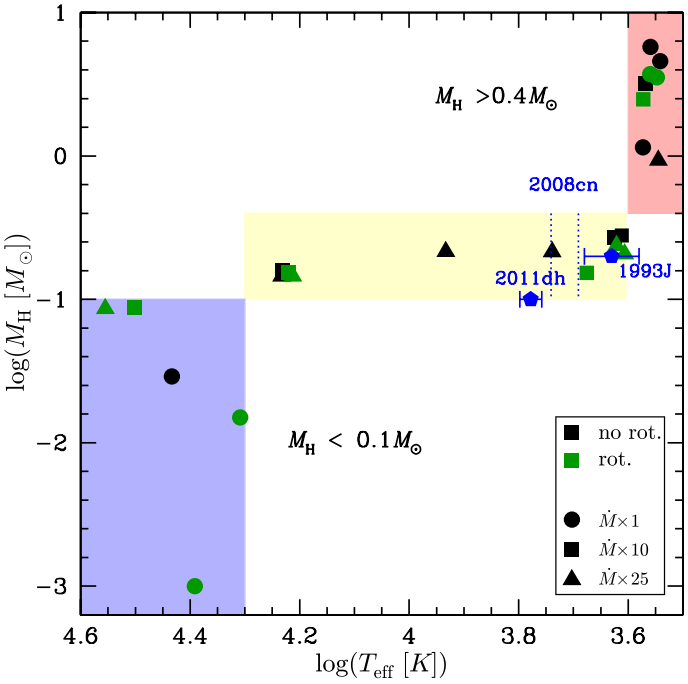

Fig. 10. Mass of hydrogen in solar masses at the pre-supernova stage for the various models of Table 1. Positions in this diagram of some supernovae are indicated by pentagons with error bars. In the case of the SN2008cn, the mass of hydrogen is not known, the range of effective temperatures is framed by the two dotted vertical segments. The three shaded regions from left to right correspond to stars ending their lifetime as blue, yellow and red supergiants.

Table 5. Properties of the last computed models with effective temperatures between 3.6 and 4.3 ordered from top to bottom by increasing effective temperatures (in logarithm). The luminosity is in logarithm, the masses in solar masses. The model nn/mm/pp corresponds to the models with an initial mass nn, a RSG mass-loss rate increased by a factor mm, and an initial rotation on the ZAMS equal to pp times the critical velocity υ_{crit}.

T_{eff}	$L/L_\odot$	Model	M_{fin}	M_α	M_{CO}	$\frac{L_H}{L_{core}}$	m_H	$\frac{m_H}{m_{He}}$
3.606	4.057	9/25/0.4	2.60	2.27	0.94	1.44	0.21	0.16
3.612	4.856	15/10/0	4.88	4.24	2.24	1.58	0.28	0.14
3.621	4.926	15/25/0.4	5.32	4.70	2.71	1.70	0.24	0.12
3.626	5.039	20/10/0	6.68	6.10	3.81	1.27	0.27	0.11
3.655	4.944	15/10/0.4	5.31	4.92	2.79	1.60	0.15	0.08
3.739	4.787	15/25/0	4.69	4.70	2.21	1.55	0.21	0.11
3.933	5.027	20/25/0	6.50	6.04	3.75	1.23	0.22	0.09
4.212	5.178	20/25/0.4	7.26	6.89	4.52	1.26	0.14	0.07
4.219	5.181	20/10/0.4	7.36	6.96	4.86	1.27	0.15	0.07
4.232	5.221	25/10/0	8.26	7.90	5.54	1.11	0.16	0.07
4.233	5.262	25/25/0	8.35	8.02	5.66	1.11	0.14	0.06

than 80% the initial mass down to only a few percents of the total initial mass! For the models with $\log T_{eff} > 4.3$, they are likely WR stars (Groh et al. 2013b) and the mass of the H-rich envelope covers a much more restricted range from 0.004% to a maximum of 1%. The pre-supernovae models with intermediate colors between the red and the blue (these are LBVs or YHGs at the pre-explosion; Groh et al. 2013b) present H-rich envelope covering the range between about 1 and 5%. So we see that whenever the H-rich envelope contains more than about 5% of the initial mass, the star will end as a red supergiant, and whenever the whole H-rich envelope is less than 1% of the total mass the star appears as a WR star before the SN. For intermediate situations, intermediate colors/effective temperatures are obtained and the star appears as an LBV or YHG at the pre-explosion stage.

– Instead of looking at the mass of the H-rich envelope, we can look at the integrated mass of hydrogen in the pre-supernova models. Fig. 10 shows the mass of hydrogen in the star at the pre-SN stage as a function of the effective temperature. All stars with a mass of hydrogen above 0.4 $M_\odot$ are red supergiants, all stars with a mass of hydrogen inferior to 0.1 $M_\odot$ appear as WR stars. Stars with intermediate values appear as LBVs/YHGs with effective temperatures between those corresponding to red supergiants and late-type WR stars.
– For those stars that have intermediate T_{eff} (LBVs and YHGs), we can wonder what is the parameter which governs the effective temperature or the total radius of the model. In Table 5 below, we have indicated for the models belonging to the yellow region of Fig. 10 various properties. Models are ordered from top to bottom by increasing effective temperatures. We see that, in general, the effective temperature increases when the actual mass, the mass of the CO, or of the He core increases. Also, generally, the effective temperature increases when the mass of hydrogen in the envelope decreases, or when the ratio of the mass of hydrogen to that of helium decreases.

Let us end this section by saying a few words about the surface rotational velocities of post RSG stars. There is a big difference between the case of the 9 $M_\odot$ model and the more massive models considered here. The rotation velocity of the 9 $M_\odot$ is higher along the blue loop than during the first crossing of the HR gap (standard mass loss rate model) . Typically at an effective temperature of Log $(T_{\rm eff}/K)$ = 3.8, the 9 $M_\odot$ model has a surface velocity of about 18 km s^{-1} during its first crossing. This velocity becomes about 106 km s^{-1} during the second crossing and nearly 43 km s^{-1} during the third crossing ! In that case, we see that from the RSG stage where the surface velocity is very small, we have a rapid increase of the surface velocity when the star contracts to the blue. Now if we consider the case of the 15 $M_\odot$ model (model with 10 times the standard mass-loss rate), we have a very different situation. At Log $(T_{\rm eff}/K)$ = 3.8, the surface rotational velocity is between 9 and 10 km s^{-1} during the first crossing, and only 0.3 and 0. 1km s^{-1} during the second and third crossing. This very different behavior results from the fact that in the 9 $M_\odot$ model, the blue ward evolution results from the mirror effect (see section 2), while for the 15 $M_\odot$, as well as for more massive stars, the blue ward evolution results from strong mass-loss. In the case of the 9 $M_\odot$ model, one has that angular momentum is dredged up to the surface by the deep convective zone during the RSG phase. This model does not lose a lot of mass (see Table 1), therefore this angular momentum remains in the star and produces an acceleration of the envelope when the star contracts to the blue (Heger & Langer 1998). In the case of the 15 $M_\odot$, the evolution to the blue part of the HR diagram is due to strong mass-losses which remove also a lot of angular moment making the surface velocities very low during the post RSG stages. So interestingly, the physical mechanism responsible for the blue ward evolution has an important impact on the surface velocities in the yellow and blue supergiant domain.

5.2. Core collapse supernovae with a post-red supergiant progenitor

Some supernovae are observed to have a yellow or a blue progenitor while being in the mass range of stars evolving into a red supergiant phase during their lifetime. Most likely these stars reach that point because they lost significant amounts of mass during the red supergiant phase. We present in Table 6, the list of known progenitors of type II supernovae for which the progenitors was not a red supergiant. Their positions in the HRD diagram are shown in Figs. 7.

Obviously, the non-rotating models with normal RSG mass-loss rate cannot account for the existence of most if not all those stars. All the observed yellow progenitors can be explained in the frame of the non-rotating models computed with some enhancement of the RSG mass-loss rates. However rotating models, with standard mass-loss rate, present blue ward evolution above a luminosity around 5.0, thus these models may be also invoked to explain some post red supergiants progenitors with luminosities above this limit[7]. Thus there is some degeneracy between the effects of rotation and those induced by different RSG mass-loss rates. Is there any possibility to discriminate between these two possibilities by observing yellow supergiants? The surface velocities in these stages are very low, so difficult to measure and moreover, their values tell very little about the initial rotation.

[7] Note that we have computed only two sets of models with different rotational velocities (0 and $0.4\upsilon_{\rm crit}$). In reality, we have a distribution of initial rotations and thus the domain of SN progenitors covered by the rotating models is larger than the one shown in the right panel of Fig. 7.

Table 6. Properties of post-RSG identified as SN progenitor. Column 1 gives the number used to label the points in Figs. 7.

	SN	type	[O/H]	Log $L/L_\odot$	Log $T_{\rm eff}$	Reference
1	1993J	II-Ib	-	5.1±0.3	3.63±0.05	[1]
2	2008cn	II-P	8.76±0.24	4.93±0.1	3.716±0.025	[2]
3	2009hd	II-L	8.43±0.05	≤5.04	≤ 3.725	[3]
4	2009kr	II-L	8.67	5.12±0.15	3.724±0.045	[4]
		IIn-II-P	8.06±0.24	5.1±0.24	3.685	[5]
5	2011dh	IIb	∼8.7	4.92±0.20	3.778±0.02	[6]
		IIb	∼8.7	4.99	3.778±0.01	[7]
6	2013df	IIb	∼8.7	4.94±0.06	3.628±0.01	[8]

Notes. [1]=Maund et al. (2004); [2]=Elias-Rosa et al. (2009); [3]=Elias-Rosa et al. (2011); [4]=Elias-Rosa et al. (2010); [5]=Fraser et al. (2010); [6]=Maund et al. (2011); [7]=Van Dyk et al. (2011); [8]=Van Dyk et al. (2014)

The surface abundances also do not appear very constraining. May be more hope can come from asteroseismology. The possibility to probe for instance the internal rotation could may be a way to differentiate between rotation or mass loss as the main cause for the existence of these yellow progenitors.

Let us now discuss each of the 6 supernovae identified as having a yellow supergiant as progenitor.

SN 1993J: this supernova originated very likely from a close binary system, consisting, a few thousand years before explosion, of a red (the primary) and a blue supergiant. Roche Lobe Overflow from the red supergiant caused its blueward evolution (Podsiadlowski et al. 1993; Maund et al. 2004). This scenario is strongly supported by the detection of the hot component of this close binary system (Maund et al. 2004). Although the present models are for single stars, the enhanced mass-loss rate models can somewhat mimic the effect of a Roche Lobe Overflow. We see that the rotating 15 $M_\odot$ model with a mass-loss increased by a factor 25 during the red supergiant stage would provide a reasonable fit to the progenitor of 1993J. The luminosity is actually 0.2 dex below the attributed luminosity but still in the error bar. Interestingly the lightcurve is well matched with models of an explosion of a He-core of mass 4-5 $M_\odot$ which had a low mass H-envelope of around 0.2 $M_\odot$ (Nomoto et al. 1993; Podsiadlowski et al. 1993; Woosley et al. 1994). Using the values of the effective temperature determined by Maund et al. (2004) as well as the mass of hydrogen in the envelope we can place the position of this SN progenitor in Fig. 10. Our rotating 15 $M_\odot$ with 25 times the standard mass-loss ends its lifetime with 5.3 $M_\odot$ and a low mass H-envelope of 0.2 $M_\odot$, the He-mass in the pre-supernova model is 1.9 $M_\odot$, its CO core mass is 2.2 $M_\odot$. So this model would provide a good fit not only to the observed position in the HR diagram but likely also for the evolution of the supernova lightcurve.

SN 2008cn: A progenitor candidate has been proposed by Elias-Rosa et al. (2009). Its yellow color (see the right panel of Fig. 7) would place it among the yellow supergiants. According to Elias-Rosa et al. (2009), it might be that the yellow progenitor could arise from the blend of two or more stars, such as a red supergiant and a brighter, blue supergiant. Actually, the fact that the light curve did appear as a type II-P plateau would favor the explosion of a red supergiant instead of a yellow one. Actually, if we take for granted that the progenitor was the yellow supergiant, then from comparisons with the present models we can deduce the following properties: a non-rotating 18 $M_\odot$ model with mass-loss increased by more than 10 times the standard mass-loss during the RSG phase could likely provide a good fit to the observed position of the progenitor. A rotating progen-

itor with masses between 15-17 $M_\odot$ with an increased mass-loss during the RSG phase (between 10 and 25 times the standard one) would likely provide a reasonable solution too. This would mean that the actual mass of the progenitor would be between 5-8 $M_\odot$, the mass of ejected hydrogen around 0.15-0.20 $M_\odot$ and that of helium around 1.9 $M_\odot$.

SN 2009hd: This object is heavily obscured by dust. Via insertion of artificial stars into the pre-SN HST images, Elias-Rosa et al. (2011) could constrain the progenitor's properties. The magnitude and color limits are compatible with a luminous red supergiant, they also allow for the possibility that the star could have been more yellow than red. Actually the point put in Figs. 7 represent the upper values for the luminosity and effective temperature. These limits are very similar to that attributed to SN 2008cn and therefore the same estimates concerning the actual mass, the masses of H and He ejected can be made (see Sect. 5.1).

SN 2009kr: Properties of the progenitors have been obtained by two teams, Elias-Rosa et al. (2010) and Fraser et al. (2010). The properties obtained by the two teams are in relatively good agreement. The only point on which a large difference exists is on the metallicity inferred for the region where the supernova occurred (see Table 6). This illustrates the fact that indeed metallicity estimates are at the moment difficult and not very reliable. Another point where the discussion between the two teams differs is on the SN type. Elias-Rosa et al. (2010) from their own analysis conclude that SN 2009kr is a type II-L supernova, while Fraser et al. (2010) reports that Tendulkar et al. (2009) indicated that SN 2009kr showed the features of a II-n SN. They also report that Steele et al. (2009) claimed SN 2009kr be a type II-P. In view of the inferred position in the HR diagram and the low mass of H that it implies, we tend to support the conclusion by Elias-Rosa et al. (2010) that we have here a type II-L SN event. As for 2009kr, positions of the progenitor in the HR diagram support the view that the star is a post red supergiant star having lost a great part of its envelope as proposed by Georgy (2012).

SN 2011dh: this supernova attracted much attention, and discussion about the nature of its progenitor has been recently resolved. Actually until recently it was uncertain whether the progenitor of this supernova was a compact or an extended star. Some authors (Arcavi et al. 2011), based on the properties of the early light curve and spectroscopy, suggested that the progenitor was a member of the compact IIb family (Chevalier & Soderberg 2010) and that the progenitor identified by Maund et al. (2011) was actually not the progenitor but possibly a companion to the progenitor or a blended source, as its radius ($\sim 10^{13}$ cm) would be highly inconsistent with constraints from their post-explosion photometric and spectroscopic data. On the other hand, Bersten et al. (2012) used a set of hydrodynamical models to study the nature of the progenitor of SN 2011dh. Their modeling suggests that a large progenitor star, with a radius about 200 $R_\odot$ is needed to reproduce the early light curve. Their model would thus support the identification of the progenitor with the yellow supergiant detected at the location of the SN event in pre-explosion images. Their model gives a mass of the ejecta to be around 2 $M_\odot$, the progenitor was composed of a helium core of 3-4 $M_\odot$ and a thin hydrogen-rich envelope of about 0.1 $M_\odot$. Actually, Van Dyk et al. (2013) have shown using HST observations of the regions of SN 2011dh about 641 days after the explosion, that the yellow supergiant has disappeared implying that this star was the progenitor of the SN. Recently a candidate for the companion of the progenitor of this supernova has been detected by Folatelli et al. (2014). From the models presented here we see that whatever cause the mass-loss, it should have been quite important to make the star to evolve at that position at the time of the supernova explosion. Actually the progenitor position would be compatible with an initial mass around 15-18 $M_\odot$ having undergone more than 10 times the standard mass-loss during the red supergiant stage. Models with rotation would favor an initial mass around 15 $M_\odot$, while non-rotating ones would favor a higher initial mass around 18 $M_\odot$. Interestingly again, non rotating as well as rotating models would predict an actual mass at that position between 4 and 6 $M_\odot$, with an hydrogen mass in the envelope around 0.2 $M_\odot$, so not so far from the estimates made by Bersten et al. (2012) on the basis of the early light curve and spectra of the SN.

SN 2013df: Van Dyk et al. (2014) analyzing archived observations of the HST obtained 14 years prior to explosion, have identified the progenitor to be a yellow supergiant. This supernova shows some similarities with SN 1993J, although with less ^{56}Ni ejected and with a progenitor more extended in radius. It is clearly of type IIb.

For some of these SNe, the enhanced mass-loss models (both rotating and non-rotating) can provide a reasonable fit not only to the observed position in the HRD but also to the masses of the progenitors and of the hydrogen and or helium as they can be deduced from the observed properties of the SN light curve. So these post RSG progenitors provide some support to the enhanced mass-loss rate models, while, as we saw in the previous section, the RSG progenitors favors more the standard mass-loss rate models.

This implies that a star with a given mass and metallicity may go through different mass-loss regimes during the RSG phase. What triggers the different mass-loss regimes may be the presence of a close companion, rotation, the presence of a magnetic field... Actually the origin of the differences are not lacking, the question which remains open is to identify them and to estimate their frequency.

6. Mass-loss rates and populations of evolved stars

When the mass-loss rate is increased during the RSG phase, we expect to observe in general a smaller number of RSG stars since the RSG lifetimes are decreased. Moreover the upper mass limit of stars spending some time in the RSG stage is decreased. This can be seen in the upper panels of Fig. 11. We see that for the standard mass-loss rates and no rotation (upper left panel), the number of red supergiants varies between 1 and 28 in a cluster of 10 000 stars with ages between about 5 and 28 Myr. When a mass-loss rate one order of magnitude greater is used during the RSG phase, we see first that red supergiants appear later than in the case of standard mass-loss, the first red supergiants appear around 8 Myr instead of 4 Myr[8]. The number expected are smaller than for the models computed with a standard mass-loss rate during the whole period between 8 and about 20 Myr. The case with an increased factor of 25 shows a qualitatively similar behavior but with a stronger decrease during the period between 8 and 20 Myr.

The two lower panels compare the predicted number ratios of RSG with MS stars (two magnitudes below the turn off) with

[8] One can wonder why changing the mass-loss rate only during the RSG phase can modify the time of appearance of the first supernovae after an instantaneous burst of star formation. The code is computing the upper mass limit of stars becoming RSGs by computing through extrapolation of the durations of the RSG phases, the lower initial mass model having a RSG lifetime equal to zero. This procedure implies that when stronger RSG mass-loss rates are used, since the RSG lifetimes are reduced, this limit is lowered and thus correspond to larger ages.

the observed numbers in a few open clusters having ages between 4 and 25 Myr. A point to keep in mind is the fact that due to the small number of stars, stochastic effects can largely blur the picture. We see that the two youngest clusters do not show any RSG populations. This may be compatible with the rotating models. The other clusters present RSG/MS ratios between 8 and 14%. These values do appear more compatible with the standard mass-loss rate models than with the increased mass-loss rates ones. Although this should be seen at the moment as a weak constraint, we can just retain at the moment that the present situation would favor, for the bulk of the RSG populations, a time-averaged mass-loss rate compatible with the standard mass-losses used by the Ekström et al. (2012) models.

Enhancing the RSG mass-loss rate increases the number ratio of blue to red supergiants. Typically, for the non-rotating (rotating) 15 $M_\odot$ model, the ratio B/R ($=(t_{B1}+t_{B2})/t_{\rm RSG}$) passes from a value equal to 0.20 (0.05) for the standard model to 0.3 (6.8) and 1.7 (6.9) for respectively the 10 and 25 $\times$ the RSG mass-loss rate models. The number of blue supergiants observed in solar metallicity clusters with mass at the turn off around 9-15 $M_\odot$ (Meylan & Maeder 1983; Eggenberger et al. 2002) is around 2. We see therefore that, if a fraction of the 15 $M_\odot$ stars would undergo stronger mass-losses during the RSG phase, then it would help in making the theoretical ratio compatible with the observed ones. However this question deserves more studies for the following reasons: 1) in the case of the 9 $M_\odot$, enhancing the mass-loss rate will actually decrease the $(t_{B1} + t_{B2})/t_{\rm RSG}$ ratio through the suppression of the blue loop; 2) we know that the enhanced mass-loss rates will likely occur only for a fraction of stars, since some core collapse progenitors are red supergiants which cannot be reproduced by RSG enhanced mass loss rate models and, as seen above, the number ratio of RSG to MS stars do appear to be better fitted by the standard mass-loss rate models; 3) finally, studies at other metallicities should be undertaken since the real challenge is not to reproduce the B/R at a given metallicity but to reproduce the general trend which is an increase of the ratio B/R with metallicity.

As we have shown, models with enhanced RSG mass-loss rate (and no other further changes as enhanced post RSG mass-loss rates) do not produce WC stars. Our models indicate that simultaneous presence of RSG and WR stars of the WN type would only occur for a very limited age range, indicating that single-aged populations showing these two population should be relatively seldom. There are indeed not many cases of single aged populations showing both red supergiants and Wolf-Rayet stars. We can cite Westerlund 1 (Clark et al. 2005, although it is so massive that not all the stars may be coeval) and clusters in the centre of the Galaxy (Figer et al. 2004; Figer 2009). Interestingly Shara et al. (2013), studying the massive star population in the ScI spiral galaxy M101 found that the spatial distributions of the WR and RSG stars near a giant star-forming complex are strikingly different. WR stars dominate the complex core, while RSG dominate the complex halo. In case this difference is linked to an age difference, it could be explained by the fact that these two populations originate from different initial mass ranges.

We mentioned above that actually models with enhanced mass-loss rates decrease the number of WR star formed (see Table 3). However the mass range considered here between 9 and 25 $M_\odot$ contributes very little to the WR population that, in the present models, come mainly from more massive stars. This is why in Fig. 11, we see no difference for what concerns the WR populations between the different models.

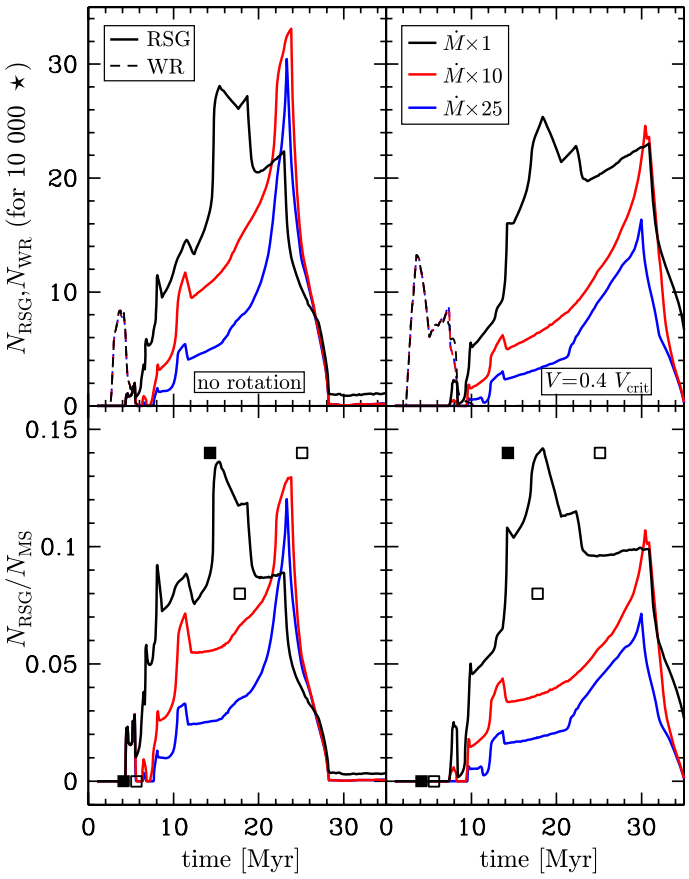

Fig. 11. *Upper panels:* Expected number of Wolf-Rayet stars (dashed lines) and of Red Supergiants in a coeval population (continuous lines) of 10000 stars. Models with initial masses between 9 and 25 $M_\odot$ computed with different mass-loss rates during the Red Supergiant phases give the different continuous lines labeled by the enhancement factor considered for the mass-loss rate during the RSG phase. The populations of WR stars are very little affected by these changes of mass-loss recipes (see text). *Lower panels:* Fraction between the number of RSG and the number of Main-Sequence stars two magnitudes below the turn off. The black and empty squares correspond to observed ratios in stellar clusters with respectively between 20 and 50 stars and with less than 20 stars. From left to right, the points correspond to the following clusters: NGC 1976, NGC 6231, NGC 884+4755, NGC 457, NGC 581+2439 (see Meynet et al. 1993).

7. Conclusions and perspectives

Red supergiants can be the end point of the evolution of massive stars or a transition phase before the star evolves into bluer parts of the HR diagram exploding when it is a yellow, a blue or even a WN-type Wolf-Rayet star. In this work, we explored how a change of the mass-loss rates during the RSG phase influences on one side the properties of the RSG and on the other side the evolution during the post RSG phases and the nature of the core collapse progenitors. The present work has reached the following conclusions:

1. For the RSG, the positions in the HRD, radii, surface abundances and rotation velocities are mostly insensitive to the RSG mass-loss rate used.
2. Adopting different mass loss rates during the RSG phase changes the initial mass attributed at a given red supergiant by evolutionary tracks. When enhanced mass loss rates are used, in general, higher initial masses are associated to a given RSG star.

3. Since the mass to be lost for a given initial mass star to leave the RSG phase is more or less fixed, enhancing the RSG mass-loss rates beyond the point making a blue ward evolution to appear, does not change the total mass lost during the RSG phase, but the duration of the RSG phase. For a star with an initial mass between 15 and 25 $M_{\odot}$, the maximum mass that can be lost during the RSG phase is between 40-60% of the initial mass.
4. A consequence of the link between RSG lifetime and mass-loss rate is that a change of the RSG mass-loss rate has a strong impact on the luminosity function of RSGs.
5. At solar metallicity, the enhanced mass-loss rate models do produce significant changes on the populations of blue, yellow and red supergiants. When extended blue loops are produced by enhanced mass-loss, the models predict that a majority of blue (yellow) supergiants are post RSG objects[9]
6. Enhanced mass-loss rates during the red supergiant phase has little impact of the WR populations. We can safely say that even the enhanced mass-loss rate models cannot reproduce the low luminosity WC stars. As indicated above post-RSG mass-loss rates during LBV's pause could help. In a work in preparation, we investigate whether these stars can be produced in close binary systems, with mass transfer occurring before the RSG phase, but this does not appear as a promiseful channel either for explaining those stars (Barblan et al. in preparation). Another possible solution would be that those stars come from massive stars with higher mass-loss rates (like in the models discussed by Maeder & Meynet 1994).
7. We show that the position in the HRD of the end point of the evolution depends on the mass of the hydrogen envelope, a point already emphasized in Groh et al. (2013b). More precisely, whenever the H-rich envelope contains more than 5% of the initial mass (actually the limit value may be between 5 and 10%) , the star will end as a red supergiant, and whenever the whole H-rich envelope is less than 1% of the total mass, the star is a blue supergiant. For intermediate situations, intermediate colors/effective temperatures are obtained.
8. An enhanced mass-loss rate during the RSG has some impact on the angular momentum of the core, but at a level which is much too low to allow this effect to be invoked for explaining the observed rotation rate of pulsars. This conclusion holds in case no other coupling than those induced by shear and meridional currents exists. In case a strong coupling would be active (due for instance to a strong magnetic coupling), then things can be very different.
9. Concerning the question, what are the RSG mass-loss rates which are favored by observations, we can bring the following elements of response: first, RSG mass-loss rates deduced from spectroscopy show a very large scatter and an outburst behavior for the mass-loss rates of RSGs. Likely, the mass lost by a star with a given initial mass and metallicity may be different depending on some additional characteristics of the star (star may have a close companion, rotation[10], ...). Arguments based on the positions of the red supergiant progenitors of type II-P supernovae and on the RSG populations in clusters indicate that the standard mass-loss rates are likely appropriate for describing the bulk of the RSG populations. On the other hand, the existence of yellow or blue progenitors with initial masses between 15 and 25 $M_{\odot}$ favors RSG enhanced mass-loss rates. Interestingly, Humphreys et al. (2013) identified stars in the galaxies M31 and M33 that they call warm hyper giants which present properties favoring a post RSG phase. These stars thus likely formed through enhanced RSG (or may be post RSG) mass-loss rates. The properties of warm hyper giants are A to F-type absorption spectra, winds with relatively slow outflows, an extensive and dusty circumstellar ejecta, and relatively high mass-loss. The warm hypergiants show the small oscillations often referred to as α Cygni variability (van Genderen & Sterken 2002). This would be exactly in line with the conclusion by Saio et al. (2013), who explain the pulsational properties of the alpha Cygni variables, which are blue supergiants with masses around 20-25 $M_{\odot}$, by the fact that they are post RSG stars (see also the discussion in Georgy et al. 2014). More work is needed to know the main physical cause(s) for enhanced RSG mass-loss rates and their frequency of occurrence.
10. The physical mechanism responsible for the blue ward evolution has an important impact on the surface velocities in the yellow and blue supergiant domain: when it is due to a mirror effect (core expansion+envelope contraction), high surface velocities are expected, while when the blue ward evolution is due to strong mass-loss, very low surface velocities are expected.

It would be interesting to explore the impact of a change of the mass-loss rate during the RSG phase at other metallicities. Actually, we can already say that models computed with the same physics as the present ones but for lower values of Z, would not much be affected by a change of the mass-loss rate during the RSG phase.The reason is that the present metal poor models burn most of the helium in the core in the blue region of the HRD (see the discussion in Georgy et al. 2013). Thus when they enter the RSG phase, they are at the end of their core helium burning stage and thus an increased mass-loss during the very short RSG phase has nearly no effect. However, Maeder & Meynet (2001) and Meynet et al. (2013) showed that for a different choice of the diffusion coefficients describing the rotational mixing, stars at low metallicity burn most of their helium in the core in the RSG phase. Enhancing the RSG mass-loss rates in those models would have impacts on the RSG lifetimes and post RSG evolution qualitatively similar to those discussed here. So we see that the discovery of yellow or blue SN progenitors at metallicities lower or equal than about Z=0.006, in the mass range between 15 and 25 $M_{\odot}$, like the progenitor of SN87A (Arnett et al. 1989), might indirectly provide some hints not only on the physics of mass-loss but also on the physics of rotational mixing!

Acknowledgements. The authors thanks Hideyuki Saio for his careful reading of the manuscript, as well as Luc Dessart and Ben Davies for interesting suggestions. G.M. acknowledges support from the Swiss National Science Foundation (project number 200020-146401) and thanks the hospitality of the Lowell Observatory where part of this work was done. C.G. acknowledges support from the European Research Council under the European Union Seventh Framework Programme (FP/2007-2013) / ERC Grant Agreement n. 306901. PM's involvement was supported by the National Science Foundation through AST-1008020.

[9] One exception however is for the rotating 20 $M_{\odot}$ for which the duration of the yellow supergiant phase before the RSG phase is longer than the duration of the same phase after the RSG phase.

[10] In the present models we have explored some effects of rotation but, for instance, the impact of rotation on the pulsation properties of red supergiants has not been studied yet. Also a strong coupling due to an internal magnetic field may bring some diversity in the evolutionary scenarios

References

Arcavi, I., Gal-Yam, A., Yaron, O., et al. 2011, ApJ, 742, L18

Arnett, W. D., Bahcall, J. N., Kirshner, R. P., & Woosley, S. E. 1989, ARA&A, 27, 629
Beck, P. G., Montalban, J., Kallinger, T., et al. 2012, Nature, 481, 55
Bersten, M. C., Benvenuto, O. G., Nomoto, K., et al. 2012, ApJ, 757, 31
Blaauw, A. 1961, Bull. Astron. Inst. Netherlands, 15, 265
Blondin, J. M. & Mezzacappa, A. 2007, Nature, 445, 58
Carr, J. S., Sellgren, K., & Balachandran, S. C. 2000, ApJ, 530, 307
Chevalier, R. A. & Soderberg, A. M. 2010, ApJ, 711, L40
Chieffi, A. & Limongi, M. 2013, ApJ, 764, 21
Choi, Y. K., Hirota, T., Honma, M., et al. 2008, PASJ, 60, 1007
Clark, J. S., Negueruela, I., Crowther, P. A., & Goodwin, S. P. 2005, A&A, 434, 949
Cox, N. L. J., Kerschbaum, F., van Marle, A.-J., et al. 2012, A&A, 537, A35
Crowther, P. A. 2001, in Astrophysics and Space Science Library, Vol. 264, The Influence of Binaries on Stellar Population Studies, ed. D. Vanbeveren, 215
Davies, B., Figer, D. F., Kudritzki, R.-P., et al. 2007, ApJ, 671, 781
Davies, B., Kudritzki, R.-P., & Figer, D. F. 2010, MNRAS, 407, 1203
Davies, B., Kudritzki, R.-P., Plez, B., et al. 2013, ApJ, 767, 3
Davies, B., Origlia, L., Kudritzki, R.-P., et al. 2009, ApJ, 694, 46
de Jager, C., Nieuwenhuijzen, H., & van der Hucht, K. A. 1988, A&AS, 72, 259
Decin, L., Hony, S., de Koter, A., et al. 2006, A&A, 456, 549
Dessart, L., Hillier, D. J., Waldman, R., & Livne, E. 2013, MNRAS, 433, 1745
Eggenberger, P., Meynet, G., & Maeder, A. 2002, A&A, 386, 576
Eggenberger, P., Montalbán, J., & Miglio, A. 2012, A&A, 544, L4
Ekström, S., Georgy, C., Eggenberger, P., et al. 2012, A&A, 537, A146
Elias-Rosa, N., Van Dyk, S. D., Li, W., et al. 2010, ApJ, 714, L254
Elias-Rosa, N., Van Dyk, S. D., Li, W., et al. 2009, ApJ, 706, 1174
Elias-Rosa, N., Van Dyk, S. D., Li, W., et al. 2011, ApJ, 742, 6
Figer, D. F. 2009, Massive-star formation in the Galactic center:, ed. M. Livio & E. Villaver, 40–59
Figer, D. F., Rich, R. M., Kim, S. S., Morris, M., & Serabyn, E. 2004, ApJ, 601, 319
Folatelli, G., Bersten, M. C., Benvenuto, O. G., et al. 2014, ApJ, 793, L22
Fraser, M., Ergon, M., Eldridge, J. J., et al. 2011, MNRAS, 417, 1417
Fraser, M., Maund, J. R., Smartt, S. J., et al. 2012, ApJ, 759, L13
Fraser, M., Maund, J. R., Smartt, S. J., et al. 2014, MNRAS, 439, L56
Fraser, M., Takáts, K., Pastorello, A., et al. 2010, ApJ, 714, L280
Georgy, C. 2012, A&A, 538, L8
Georgy, C., Ekström, S., Eggenberger, P., et al. 2013, A&A, 558, A103
Georgy, C., Ekström, S., Meynet, G., et al. 2012, A&A, 542, A29
Georgy, C., Saio, H., & Meynet, G. 2014, MNRAS, 439, L6
Giannone, P. 1967, ZAp, 65, 226
Groh, J. H., Meynet, G., & Ekström, S. 2013a, A&A, 550, L7
Groh, J. H., Meynet, G., Ekström, S., & Georgy, C. 2014, A&A, 564, A30
Groh, J. H., Meynet, G., Georgy, C., & Ekström, S. 2013b, A&A, 558, A131
Gvaramadze, V. V., Menten, K. M., Kniazev, A. Y., et al. 2014, MNRAS, 437, 843
Heger, A. & Langer, N. 1998, A&A, 334, 210
Heger, A., Woosley, S. E., & Spruit, H. C. 2005, ApJ, 626, 350
Hinkle, K. H., Lambert, D. L., & Snell, R. L. 1976, ApJ, 210, 684
Humphreys, R. M., Davidson, K., Grammer, S., et al. 2013, ApJ, 773, 46
Humphreys, R. M., Helton, L. A., & Jones, T. J. 2007, AJ, 133, 2716
Jerkstrand, A., Fransson, C., Maguire, K., et al. 2012, A&A, 546, A28
Josselin, E., Blommaert, J. A. D. L., Groenewegen, M. A. T., Omont, A., & Li, F. L. 2000, A&A, 357, 225
Jura, M. & Kleinmann, S. G. 1990, ApJS, 73, 769
Lambert, D. L., Brown, J. A., Hinkle, K. H., & Johnson, H. R. 1984, ApJ, 284, 223
Lauterborn, D., Refsdal, S., & Weigert, A. 1971, A&A, 10, 97
Levesque, E. M., Massey, P., Olsen, K. A. G., et al. 2005, ApJ, 628, 973
Levesque, E. M., Massey, P., Olsen, K. A. G., et al. 2006, ApJ, 645, 1102
Maeder, A. 1997, A&A, 321, 134
Maeder, A. 2009, Physics, Formation and Evolution of Rotating Stars
Maeder, A. & Meynet, G. 1987, A&A, 182, 243
Maeder, A. & Meynet, G. 1994, A&A, 287, 803
Maeder, A. & Meynet, G. 2000, A&A, 361, 159
Maeder, A. & Meynet, G. 2001, A&A, 373, 555
Maeder, A., Przybilla, N., Nieva, M.-F., et al. 2014, A&A, 565, A39
Marques, J. P., Goupil, M. J., Lebreton, Y., et al. 2013, A&A, 549, A74
Massey, P., Silva, D. R., Levesque, E. M., et al. 2009, ApJ, 703, 420
Matsuura, M., Yates, J. A., Barlow, M. J., et al. 2014, MNRAS, 437, 532
Maund, J. R., Fraser, M., Ergon, M., et al. 2011, ApJ, 739, L37
Maund, J. R., Mattila, S., Ramirez-Ruiz, E., & Eldridge, J. J. 2014, MNRAS, 438, 1577
Maund, J. R., Smartt, S. J., Kudritzki, R. P., Podsiadlowski, P., & Gilmore, G. F. 2004, Nature, 427, 129
Mauron, N. & Josselin, E. 2011, A&A, 526, A156
Meylan, G. & Maeder, A. 1983, A&A, 124, 84
Meynet, G., Ekstrom, S., Maeder, A., et al. 2013, in Lecture Notes in Physics, Berlin Springer Verlag, Vol. 865, Lecture Notes in Physics, Berlin Springer Verlag, ed. M. Goupil, K. Belkacem, C. Neiner, F. Lignières, & J. J. Green, 3–642
Meynet, G., Mermilliod, J.-C., & Maeder, A. 1993, A&AS, 98, 477
Nomoto, K., Suzuki, T., Shigeyama, T., et al. 1993, Nature, 364, 507
Noriega-Crespo, A., van Buren, D., Cao, Y., & Dgani, R. 1997, AJ, 114, 837
Origlia, L., Oliva, E., Maiolino, R., et al. 2013, A&A, 560, A46
Podsiadlowski, P., Hsu, J. J. L., Joss, P. C., & Ross, R. R. 1993, Nature, 364, 509
Poveda, A., Ruiz, J., & Allen, C. 1967, Boletin de los Observatorios Tonantzintla y Tacubaya, 4, 86
Przybilla, N., Firnstein, M., Nieva, M. F., Meynet, G., & Maeder, A. 2010, A&A, 517, A38
Saio, H., Georgy, C., & Meynet, G. 2013, MNRAS, 433, 1246
Salasnich, B., Bressan, A., & Chiosi, C. 1999, A&A, 342, 131
Sander, A., Hamann, W.-R., & Todt, H. 2012, A&A, 540, A144
Shara, M. M., Bibby, J. L., Zurek, D., et al. 2013, AJ, 146, 162
Smartt, S. J. 2009, ARA&A, 47, 63
Smith, N., Humphreys, R. M., Davidson, K., et al. 2001, AJ, 121, 1111
Smith, N., Li, W., Filippenko, A. V., & Chornock, R. 2011, MNRAS, 412, 1522
Steele, T. N., Cobb, B., & Filippenko, A. V. 2009, Central Bureau Electronic Telegrams, 2011, 1
Stone, R. C. 1991, AJ, 102, 333
Sylvester, R. J., Skinner, C. J., & Barlow, M. J. 1998, MNRAS, 301, 1083
Tendulkar, S. P., Kasliwal, M. M., Quimby, R., & Kulkarni, S. R. 2009, The Astronomer's Telegram, 2291, 1
Tomasella, L., Cappellaro, E., Fraser, M., et al. 2013, MNRAS, 434, 1636
Uitenbroek, H., Dupree, A. K., & Gilliland, R. L. 1998, AJ, 116, 2501
van Belle, G. T., Creech-Eakman, M. J., & Hart, A. 2009, MNRAS, 394, 1925
Van Dyk, S. D., Cenko, S. B., Poznanski, D., et al. 2012a, ApJ, 756, 131
Van Dyk, S. D., Davidge, T. J., Elias-Rosa, N., et al. 2012b, AJ, 143, 19
Van Dyk, S. D., Li, W., Cenko, S. B., et al. 2011, ApJ, 741, L28
Van Dyk, S. D., Zheng, W., Clubb, K. I., et al. 2013, ApJ, 772, L32
Van Dyk, S. D., Zheng, W., Fox, O. D., et al. 2014, AJ, 147, 37
van Genderen, A. M. & Sterken, C. 2002, A&A, 386, 926
van Loon, J. T., Cioni, M.-R. L., Zijlstra, A. A., & Loup, C. 2005, A&A, 438, 273
van Loon, J. T., Groenewegen, M. A. T., de Koter, A., et al. 1999, A&A, 351, 559
Vanbeveren, D., Van Bever, J., & Belkus, H. 2007, ApJ, 662, L107
Vink, J. S., de Koter, A., & Lamers, H. J. G. L. M. 2001, A&A, 369, 574
Woosley, S. E., Eastman, R. G., Weaver, T. A., & Pinto, P. A. 1994, ApJ, 429, 300
Yoon, S.-C. & Cantiello, M. 2010, ApJ, 717, L62
Zahn, J.-P. 1992, A&A, 265, 115